Accepted Manuscript

Rescuing the CFTR protein function: Introducing 1,3,4-oxadiazoles as translational readthrough inducing drugs

Ivana Pibiri, Laura Lentini, Raffaella Melfi, Marco Tutone, Sara Baldassano, Paola Ricco Galluzzo, Aldo Di Leonardo, Andrea Pace

PII: S0223-5234(18)30835-3

DOI: 10.1016/j.ejmech.2018.09.057

Reference: EJMECH 10768

To appear in: *European Journal of Medicinal Chemistry*

Received Date: 10 August 2018

Revised Date: 21 September 2018

Accepted Date: 24 September 2018

Please cite this article as: I. Pibiri, L. Lentini, R. Melfi, M. Tutone, S. Baldassano, P.R. Galluzzo, A. Di Leonardo, A. Pace, Rescuing the CFTR protein function: Introducing 1,3,4-oxadiazoles as translational readthrough inducing drugs, *European Journal of Medicinal Chemistry* (2018), doi: https://doi.org/10.1016/j.ejmech.2018.09.057.

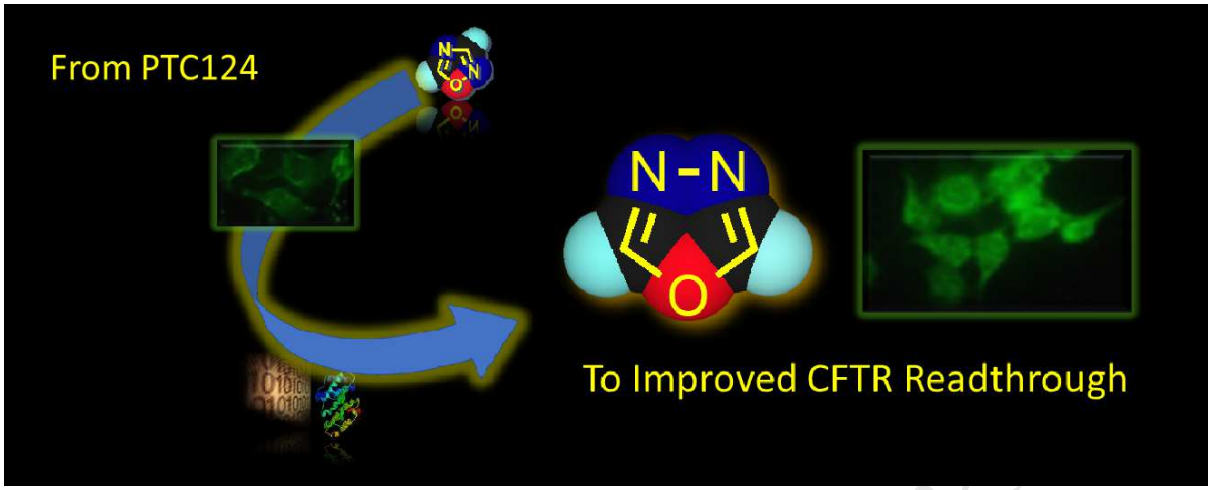

Rescuing the CFTR protein function: introducing 1,3,4-oxadiazoles as translational readthrough inducing drugs

Ivana Pibiri[*‡a], Laura Lentini*[*‡a], Raffaella Melfi*[a], Marco Tutone*[a], Sara Baldassano*[a], Paola Ricco Galluzzo*[a], Aldo Di Leonardo*[a,b] and Andrea Pace*[a]

[a]Dipartimento di Scienze e Tecnologie Biologiche, Chimiche e Farmaceutiche (STEBICEF), Università degli Studi di Palermo, Viale delle Scienze Ed. 16-17, 90128, Palermo, Italy. [b]Centro di OncoBiologia Sperimentale (COBS) via San Lorenzo Colli 90145 Palermo, Italy.

KEYWORDS. *Cystic Fibrosis, Premature Termination Codon, Nonsense Mutation, Genetic Disorder, Oxadiazole.*

ABSTRACT. [1]Nonsense mutations in the CFTR gene prematurely terminate translation of the CFTR mRNA leading to the production of a truncated protein that lacks normal function causing a more severe form of the cystic fibrosis (CF) disease. About 10% of patients affected by CF

ABBREVIATIONS: CCR2, CC chemokine receptor 2; CCL2, CC chemokine ligand 2; CCR5, CC chemokine receptor 5; TLC, thin layer chromatography.

show a nonsense mutation. A potential treatment of this alteration is to promote translational readthrough of premature termination codons (PTCs) by Translational Readthrough Inducing Drugs (TRIDs) such as PTC124. In this context we aimed to compare the activity of PTC124 with analogues differing in the heteroatoms position in the central heterocyclic core. By a validated protocol consisting of computational screening, synthesis and biological tests we identified a new small molecule (**NV2445)** with 1,3,4-oxadiazole core showing a high readthrough activity. Moreover, we evaluated the CFTR functionality after **NV2445** treatment in CF model systems and in cells expressing a *nonsense*-CFTR-mRNA. Finally, we studied the supramolecular interactions between TRIDs and CFTR-mRNA to assess the biological target/mechanism and compared the predicted ADME properties of **NV2445** and PTC124.

INTRODUCTION

Cystic fibrosis (CF) is caused by mutations in the gene encoding the cystic fibrosis trans-membrane conductance regulator (CFTR). About 2000 different mutations are involved in the CF pathology [1], the most common being a three base pair deletion causing the loss of phenylalanine at position 508 (ΔF508) and a missense mutation at position 551 (G551D). Nonsense-mutations in the CFTR gene represent approximately 10% of the CF cases, their presence produce a truncated protein that is rapidly degraded, so the patients lack the functional protein and suffer a more severe form of the disease.

Pharmaceutical approaches targeting the specific genetic defect have been faced and heterocyclic scaffolds rule the personalized medicinal approach, as proved by many studies in the CF field [2-6].

Concerning *nonsense* mutations, in the last ten years the only treatment proposed for these patients was the *translational readthrough* of the premature termination codon (PTC) to selectively promote the bypass of the PTC so that the expression of a functional protein is restored to some extent. To this aim aminoglycosides (e.g. gentamicin, tobramycin, paromomycin, geneticin reported in Figure 1) were previously used to suppress the normal proof-reading function of the ribosome [7,8] leading to the insertion of a near-cognate amino acid at the PTC site thus allowing the translation of the remainder of the open reading frame. However, severe side-effects caused by prolonged treatments with aminoglycosides including renal, auditory, and vestibular toxicities have been reported [9], limiting their widespread clinical use for this purpose. Despite these issues, very recently a new aminoglycoside showed potential activity as TRID and was launched in phase II clinical trials [10].

PTC124 (Figure 1), also known as Ataluren, was launched by PTC Therapeutics to promote the readthrough of premature but not normal termination codons in HEK293 cells [11]. PTC124 does not possess the toxicity of an aminoglycoside and has been suggested as a potential treatment of genetic disorders caused by nonsense mutations, particularly those involving the UGA premature codon [12]. Although results of the phase II studies showed improvement in markers of CFTR function, no improvements in sweat chloride levels or nasal potential difference were reported in a new phase III trial [13]. In May 2014, PTC Therapeutics concluded phase III Clinical trials for FC and DMD patients, in order to evaluate long-term safety of PTC124 and supported the registration of the drug to the regulatory authorities. At conclusion of this study it was evidenced that, although Ataluren (PTC124) did not improve lung function in the overall population of nonsense-mutation cystic fibrosis patients who received this treatment, it can be considered beneficial for patients not taking chronic inhaled tobramycin. The

researchers' hypothesis was that PTC124 and tobramycin, both by acting at the level of the ribosome are in competition with each other. To confirm these data an additional confirmation Phase III clinical study was started but it was suspended in April 2017 due to conflicting results [14, 15]. Therefore, today, Ataluren is among the prospective lead-like compounds despite its real efficacy in CF patients and its effective biological target are still not clear [16].

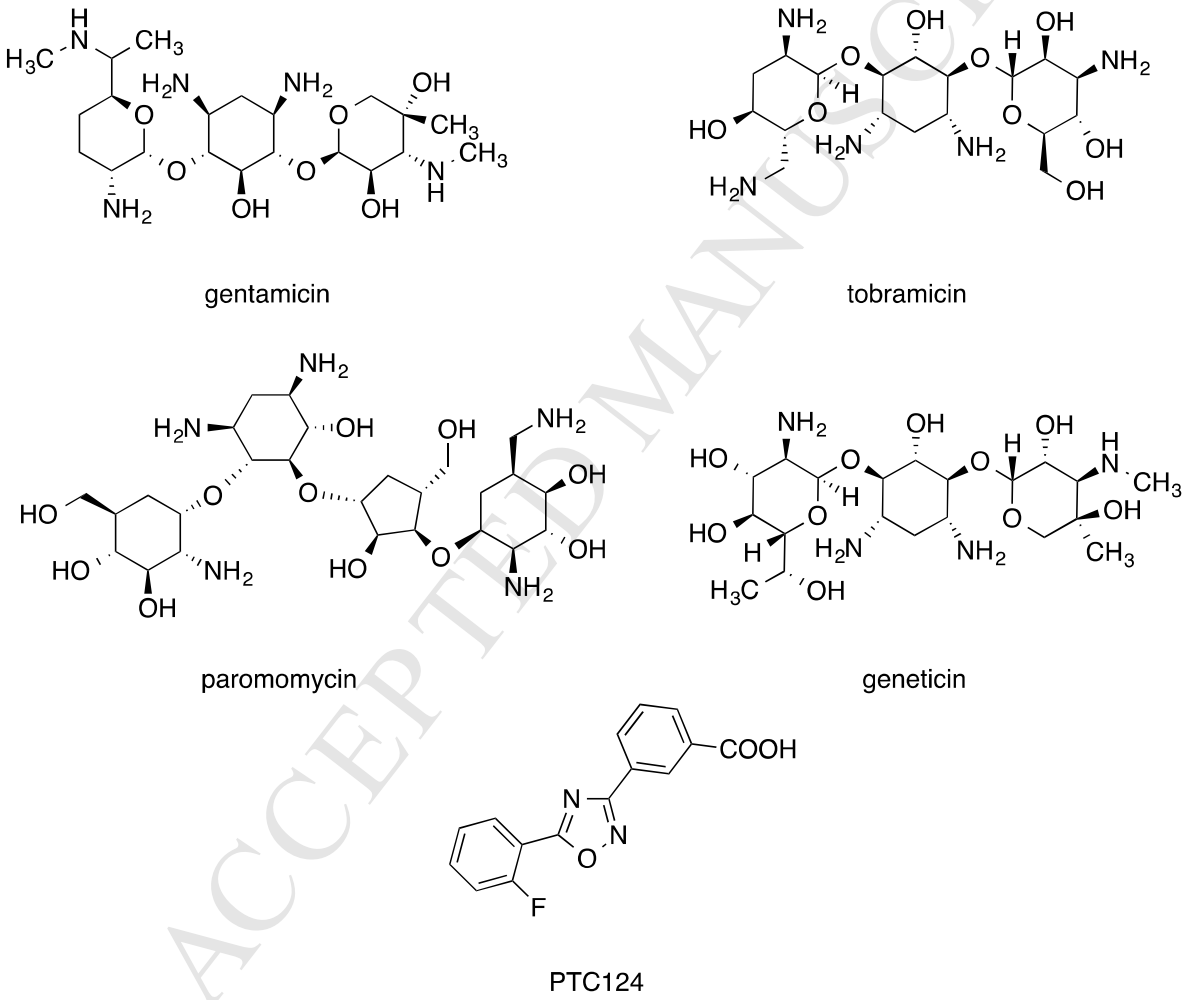

Figure 1. Structures of reported Translational Readthrough Inducing Drugs

Our previous results obtained by virtual mutagenesis of the CFTR mRNA and molecular dynamic simulation in presence of PTC124, indicated that the bases surrounding the premature stop codon in the mRNA could affect the readthrough mechanism [17, 18]. Indeed, we hypothesized that PTC124 could interact differently with different type of *nonsense* mutations of the CFTR gene (G542X, R1162X, W1282X etc.) depending on the genetic context. These observations could explain why the efficacy of PTC124 in CF is still debated and highlights the importance of the identification of new readthrough agents.

Oxadiazoles are one of the main characters in the drug discovery scene; being often used as bioisosteric replacements for ester and amide functionalities. In a work by Boström et al. [19] comparing 1,2,4- and 1,3,4-oxadiazoles, it has been shown a systematic trend, regardless of substitution patterns, in the pharmaceutical properties of these two closely related molecules. In virtually all cases, the 1,3,4-oxadiazole isomer shows an order of magnitude lower lipophilicity, increased aqueous solubility, decreased hERG inhibition, and improved metabolic stability as compared to the 1,2,4 isomer. In this context, considering that PTC124 has a 1,2,4-oxadiazole as a core, we performed a virtual screening on public and in-house structure libraries and focused further experimental studies on a selected set of small molecules containing a 1,3,4-oxadiazole heterocyclic core.

Further selection was based on biological screening using the firefly luciferase reporter, while the activity of the most promising compound as readthrough promoter was confirmed by orthogonal assays. Further computational studies simulated the interactions of the most active molecule with the specific PTC on the mRNA and predicted ADME properties.

Finally, further in vitro assays were performed to evaluate the efficacy of the most active among the synthesized compounds in re-establishing the production of a functional CFTR

protein in cells engineered to express a nonsense CFTR mRNA relative to the G542X mutation as well as in immortalized and primary cells isolated from cystic fibrosis patients.

RESULTS AND DISCUSSION

Virtual Screening. The virtual screening campaign started with the development of pharmacophore models on the basis of previous results [20] and with the refinement of obtained models by means of 3D-QSAR (quantitative structure-activity relationships) analysis. The endpoint to build QSAR models were the firefly luciferase activity (FLuc) data converted to logFLuc values (Table 1). In order to find the common pharmacophore hypothesis, we divided a set of twenty-four compounds in three sub-sets of different ranges of logFLuc activity values (Pharm set). We considered as active compounds those with logFLuc values higher than the value found for PTC124 (logFLuc > 4.528); as inactive compounds those with logFLuc $\leq$ 4.181, and as compounds of moderate activity, those with 4.182 $\leq$ logFLuc < 4.527 (Table 1). The entire Pharm set was randomly split into a training set (19 compounds) for the generation of model hypotheses (Hypo), and a test set (5 compounds) for the validation of the developed model, as reported in Table 1.

Table 1. Pharm set for pharmacophore model development

Compound	QSAR set	logFLuc RLU values Exp.	RLU values Pred.	Pharm Set	Fitness
PTC124	Test	4.528	4.58	Active	3.00
1-NV1103	Training	4.532	4.41	Active	2.94
2-NV1127	Training	4.477	4.27	Moderate	2.79
3-NV1133	Training	4.628	4.64	Active	2.82
4-NV1128	Test	4.397	4.40	Moderate	2.87
5-NV1173	Training	4.788	4.80	Active	2.90
6-NV1153	Training	4.125	4.21	Inactive	2.78
7-NV1149	Training	4.103	4.32	Inactive	2.91
8-NV1170	Training	4.311	4.42	Moderate	2.91
9-NV1175	Training	4.269	4.23	Moderate	2.76
10-NV1171	Training	4.439	4.39	Moderate	2.90
11-NV1174	Training	4.414	4.31	Moderate	2.80
12-NV1798	Training	4.178	4.18	Inactive	1.65
13-NV1751	Training	4.008	4.09	Inactive	2.71
14-NV1954	Test	4.171	4.25	Inactive	2.74
15-NV1859	Training	4.363	4.25	Moderate	2.77
16-NV1861	Training	4.250	4.24	Moderate	2.76
17-NV1879	Training	4.411	4.40	Moderate	2.78
18-NV1883	Training	4.428	4.37	Moderate	2.76
19-NV1894	Test	4.250	4.37	Moderate	2.78
20-NV1905	Training	4.181	4.19	Inactive	2.74
21-NV1898	Training	4.551	4.54	Active	2.76
22-NV1919	Test	4.253	4.27	Moderate	2.80
23-NV1940	Training	4.000	3.99	Inactive	1.66

Table 2. Statistical parameters for Hypo models comparison.

Model ID	R^2	SD	F	RMSE	Pearson-R	Q^2	Q^2 ext	R^2_0	R'^2_0	R^2_m	$(R^2-R^2_0)/R^2$	$(R^2-R'^2_0)/R^2$	k	k ‘
Hypo.7	0.805	0.102	20.7	0.0672	0.9482	0.72	0.714	0.851	0.821	0.617	-0.064	-0.026	0.987	1.012
Hypo.8	0.798	0.104	19.8	0.0941	0.9077	0.451	0.611	1.263	0.708	0.253	-0.583	0.112	0.982	1.017

SD: standard deviation; F: Fisher test; RMSE: root mean square error.

The models have been robustly validated (Table 2), and Hypo.7 showed the best predictive capability (Figure 2 and 3).

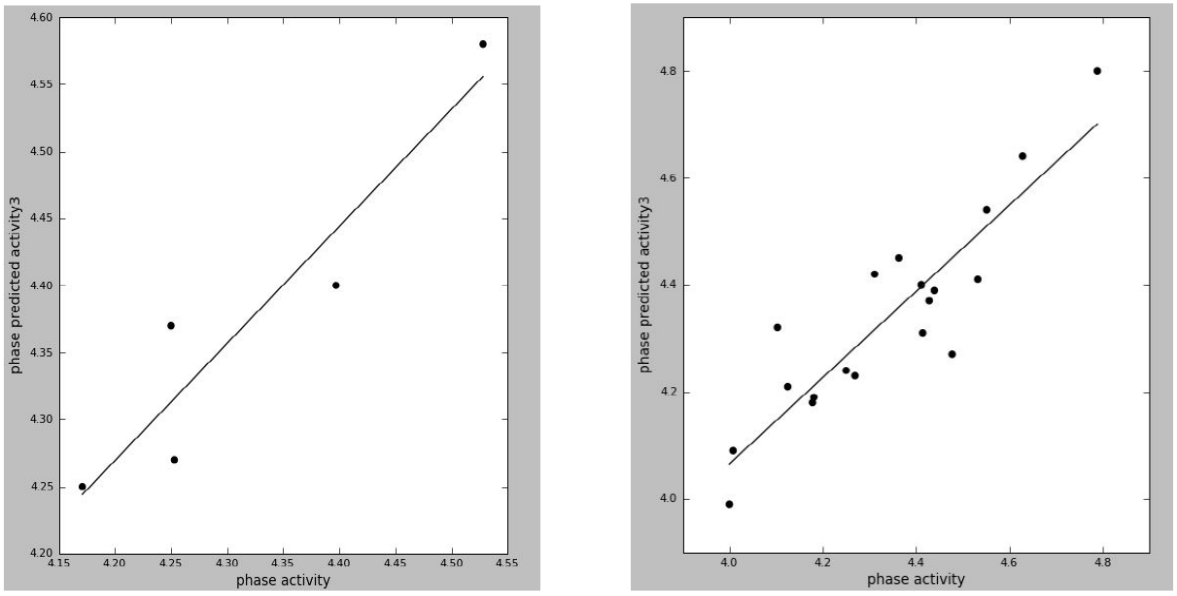

Figure 2. Test-set (left) and training-set (right) plots for Hypo.7

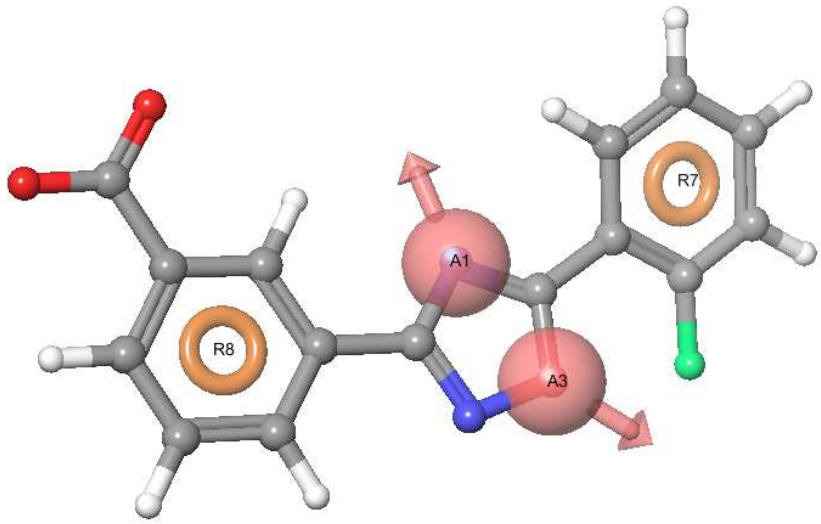

Figure 3. Validated Hypo.7 aligned with PTC124

Hypo.7 has been used as starting point to perform a high-throughput virtual screening on public databases together with an "in-house" library of compounds available in our laboratories. From the top 5% of Hypo.7 retrieved hits, we selected seven synthetically accessible 1,3,4-oxadiazoles to which we added 2-amino-5-methyl-1,3,4-oxadiazole (NV924) as a representative non-arylated 1,3,4-oxadiazole with apolar (CH_3) and H-bond acceptor/donor (NH_2) substituents (Figure 4).

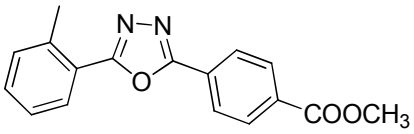

NV2347

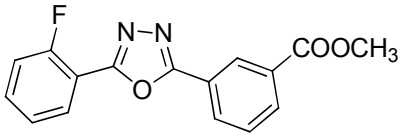

NV2653

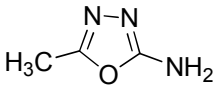

NV924

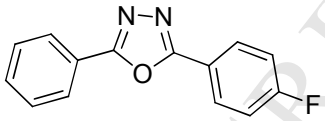

NV1191

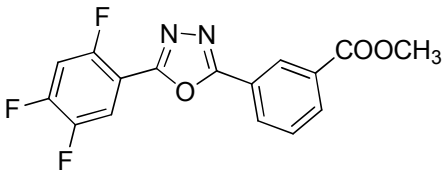

NV2712

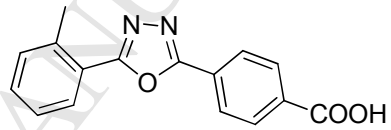

NV2445

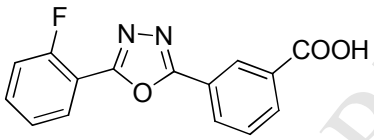

NV2702

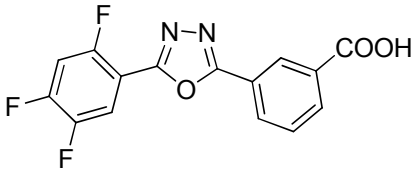

NV2729

Figure 4. Selected set of synthetically accessible 1,3,4-oxadiazoles

Synthesis. The synthetic protocol used to obtain compounds having as common feature the 1,3,4-oxadiazole core is the following (see Scheme 1): The first step is a solvent free reaction performed in a microwave oven at 900W, by reacting substituted-benzoic acid with hydrazine. In

a following step the so obtained products were further reacted with the appropriate aldehyde in refluxing ethanol, finally cyclization at 100°C was realized by stirring the open-chain compounds in the presence of molecular iodine and potassium carbonate in DMSO. In the case of ester compounds, further hydrolysis with lithium hydroxide in THF produced the corresponding acids.

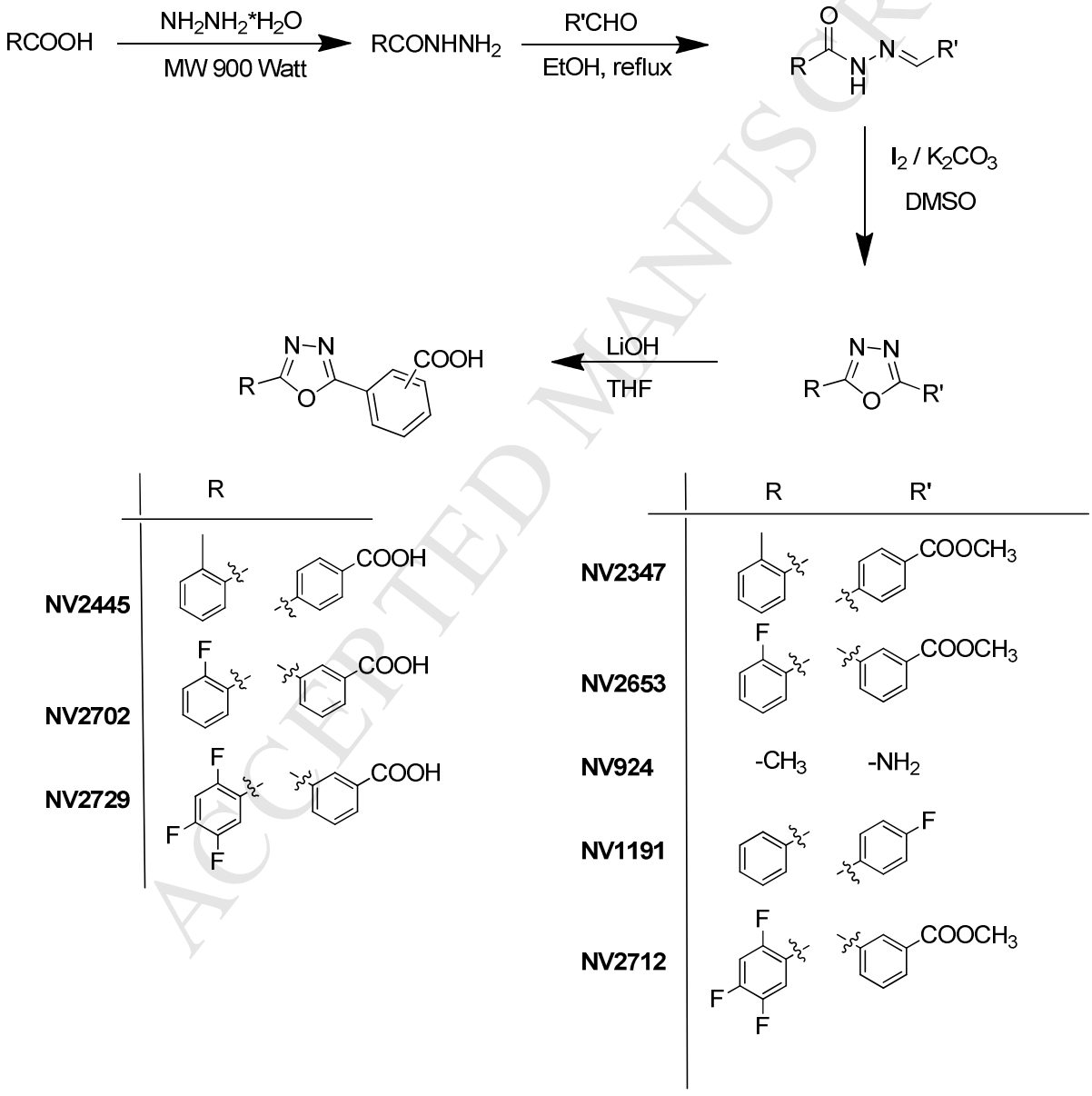

Scheme 1. Synthetic path to 1,3,4-oxadiazoles

Experimental screening of the readthrough activity by the FLuc assay. To ascertain the effectiveness of the newly synthesized PTC124 analogues in promoting the readthrough of premature termination codons we used the FLuc cell-based assay [17, 18]. To this aim HeLa cells were transfected transiently with the plasmids pFLuc-WT (control) and pFLuc-opal (UGA stop mutation) [20]. FLuc gene expression was then measured by luminescence. HeLa cells transfected with the pFluc-WT plasmid showed high levels of luciferase activity confirming the functioning of the assay (Figure 5). On the contrary, pFluc-opal transfected HeLa cells did not show any activity. However, when these pFluc-opal cells were treated with PTC124 and 8 different analogues we observed a significant increase of luciferase activity in comparison to untreated cells specifically with the analogues: NV2445>NV2712>2347 (**Figure 5**).

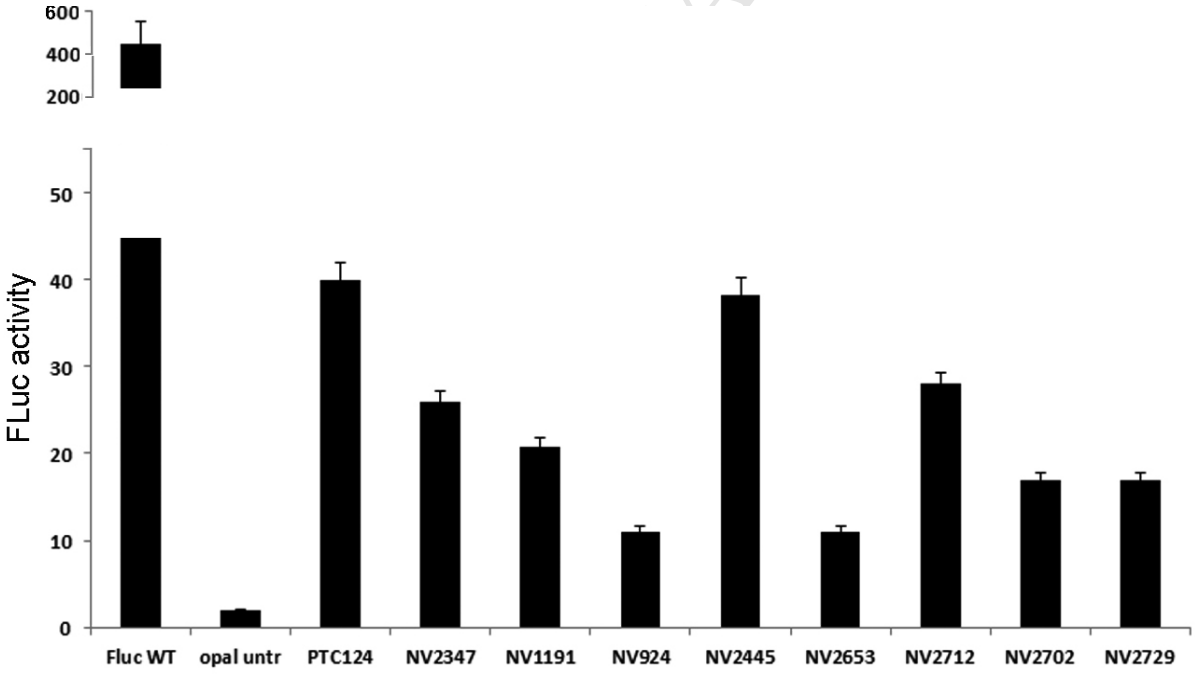

Figure 5. The new synthetized molecules show readthrough activity in FLuc cell model system. Histogram showing luciferase (FLuc) activity after 24 hours of exposition to PTC124 and its analogues (all at the concentration of 12 μM) in HeLa FLuc-opal transfected cells.

Next, we focused on the compound NV2445 that showed enhanced readthrough activity. To confirm the results for NV2445 we used HeLa cells stably transfected with a vector harboring the UGA mutation in the coding sequence of the H2BGFP cDNA [21]. Detection of green fluorescent cells after 24 hours of treatment indicates that NV2445, allows PTCs readthrough and the translation of the full length H2B-GFP fusion protein. PTC124 and G418 were used as positive control (Figure 6).

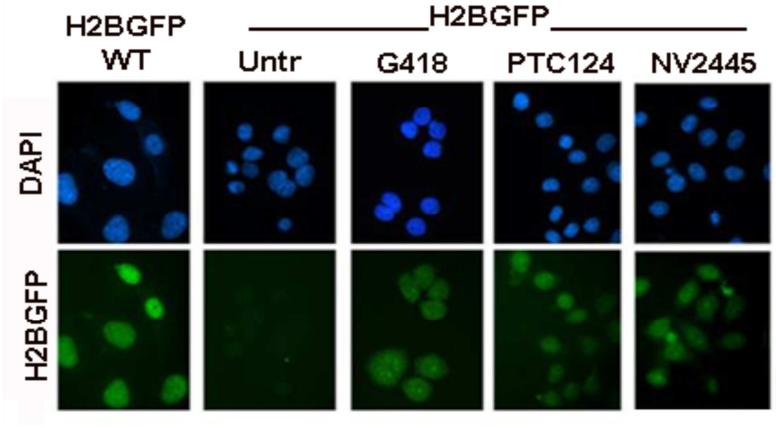

Figure 6. NV2445 induces H2BGFP expression. Immunofluorescence analysis of the H2BGFP fusion protein in H2BGFP-Opal transfected HeLa cells after 24 hours of exposition to PTC124, G418 (positive controls) and the newly synthesized molecule NV2445.

Induced Fit Docking and Molecular Dynamics on NV2445-mRNA. Similarly, to our previous study [21], and based on the experimental data obtained in this work, we decided to perform computational simulations modeling the interaction of a 33-nucleotides CFTR mRNA fragment, harboring a UGA premature stop codon, with NV2445. Induced Fit docking run followed by a 100 ns MD simulation were performed. In the Induced Fit docking (IFD) analysis, the docking box was centered on the equilibrium pose of PTC124 extracted from our previous MD study [21]. Obtained results from IFD showed as NV2445 pose is similar to PTC124 with some

difference in terms of interactions. In fact, despite PTC124-mRNA interaction is stabilized by a H-bond with A18, NV2445 establishes H-bond with U12. π-π stacking between G10 and the three aromatic rings of NV2445, and G17-1,3,4-oxadiazole ring, are the essential interactions. Despite these different binding modes, docking scores of the two molecules are almost equal (Δdocking score = 0.6 kcal/mol) (Figure 7).

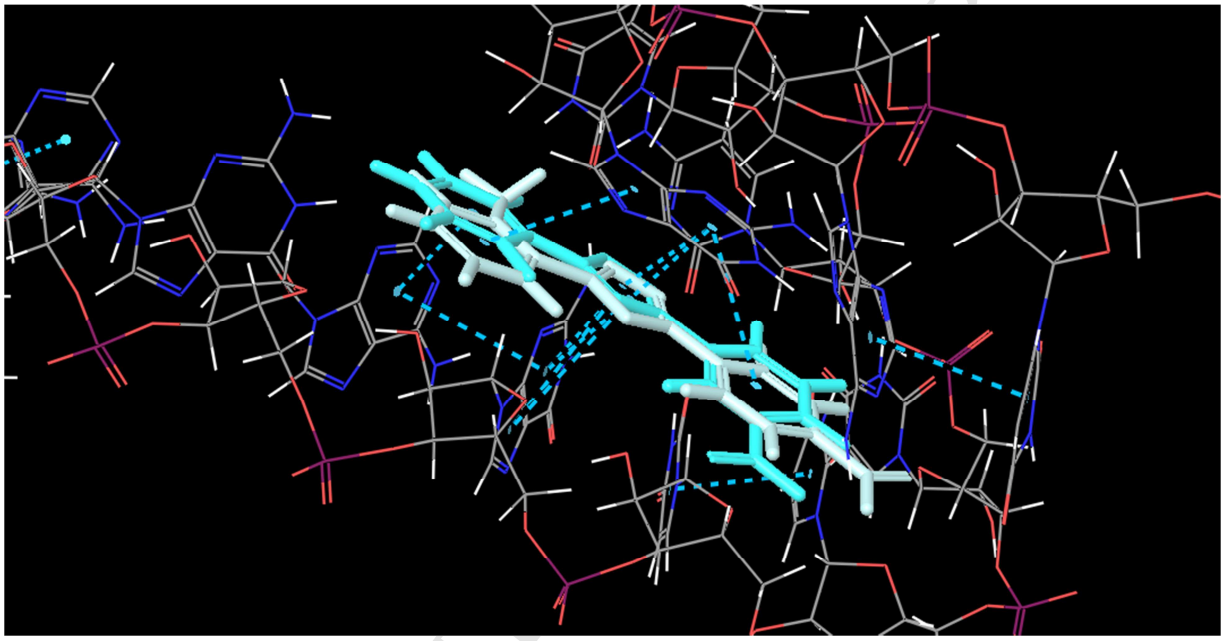

Figure 7. IFD poses of NV2445 (light blue) compared with PTC124 equilibrium pose (grey). Dashed light blue lines represent the π-π stacking interaction.

With the aim to explore how the NV2445-mRNA interactions vary during the time, and to compare with our previous study, we performed 100ns MD run starting from the NV2445 pose obtained by means of IFD. NV2445 remains in the RNA loop for the whole simulation time. Nevertheless, we observed a particular behavior of NV2445, with substantial difference from PTC124 with the UGA stop codon. After about 1 ns, NV2445 moves inside the nucleotide sequence, assuming a parallel pose among A18 and G19. This orientation of NV2445 is

maintained along the rest of the simulation, stabilized by π-π stacking occurring between the aryl moiety bearing the carboxyl group and A18, and between the tolyl moiety with G19. This particular pose puts the carboxyl group directed towards the phosphate chain, establishing H-bonding with the water molecules. While the oxadiazole ring remains in close contact with A18. In a such orientation the nitrogens of the 1,3,4-oxadiazole moiety are in close contact with the N1 and the amino group of the adenine 18, which are responsible of the H-bonds that guarantee the anticodon recognition (Figure 8).

This insertion could primarily lead to mRNA:tRNA mispairing at codon position 3 and reflects the proposed mechanism of action for PTC124 by Jacobson and coworkers [22]. In fact, they experimentally proved mispairing and insertion of the near-cognate tRNA, in particular, they demonstrated that, at position 3, multiple nonstandard mispairings are tolerated including A-C, G-G, A-G, and possibly others.

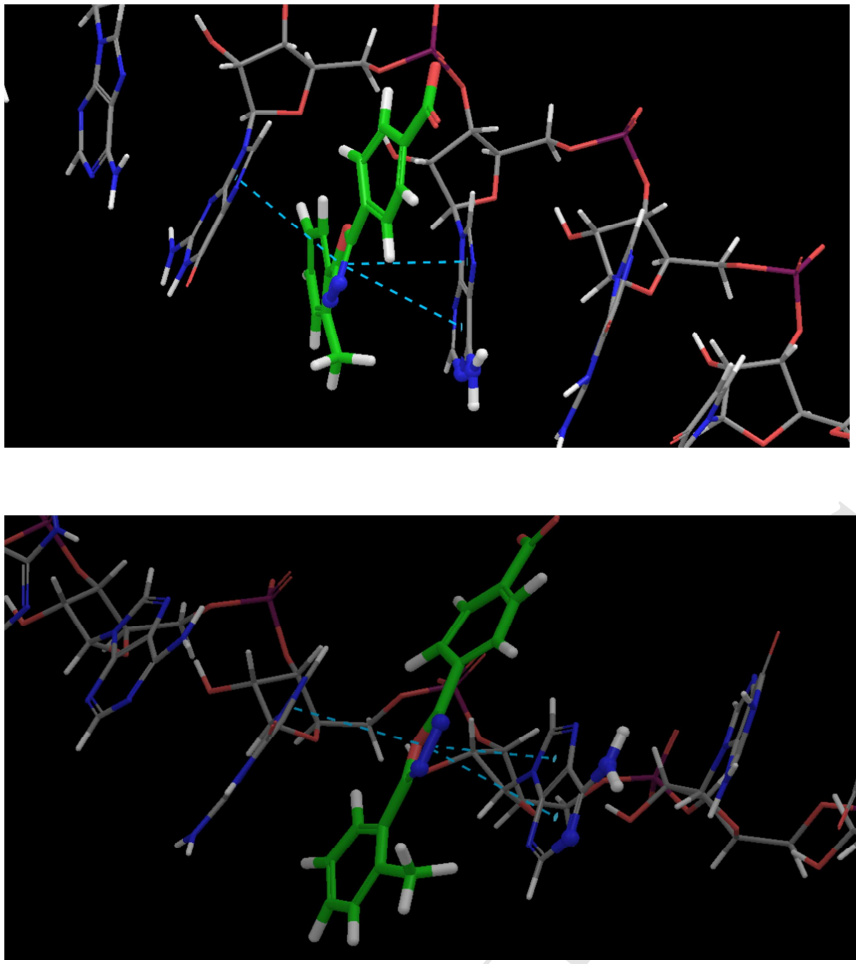

Figure 8. MD snapshots of NV2445 inserted into A18 and G19 of the mRNA. Dashed light blue lines represent the π-π stacking interactions.

We extended our investigation with the MM-GBSA calculations to get quantitative estimates for the binding free energies of the NV2445-mRNA complex compared with PTC124-mRNA complex. By means of such analysis, we are able to evaluate the free energy components such as van der Waals (vdW), electrostatic, and solvation contributions to provide detailed molecular information regarding the complexes under investigation (Table 3). The analysis of the MM-GBSA terms indicates that, even though, the two compounds have high similarity (shape similarity = 0.83) the physico-chemical properties that have a preponderant role in the potency

are quite different. For PTC124, vdW and electrostatic contributes are prominent, while for NV2445, vdW is prominent but the major contribute is due to solvation term as observed by the H-bonding of carboxyl group with water molecules. However, the binding affinity can be the result of the combination of the particular effect of these features.

Table 3. Predicted free-energies (kcal/mol) and individual energy terms of mRNA-NV2445/PTC124 complexes

Molecule	**ΔG_{calc}**	**ΔG_{vdW}**	**ΔG_{Coul}**	**ΔG_{solv}**	**$\Delta\Delta$Gcalc**
NV2445	-14.638	-24.554	98.285	-89.253	-1.213
PTC124	-13.425	-13.994	-16.292	15.821	ref

ADME-Tox predictions for NV2445. In the attempt to predict absorption, distribution, metabolism, and excretion (ADME) for NV2445, this one was submitted to Qikprop calculations and toxicity prediction such as physics-based membrane permeability and structure based P450 sites of metabolism prediction. Regarding ADME predictions the final result is expressed in terms of #stars, Number of property or descriptor values that fall outside the 95% range of similar values for known drugs large number of stars suggests that a molecule is less drug-like than molecules with few stars. The following properties and descriptors are included in the determination of #stars: MW, dipole, IP, EA, SASA, FOSA, FISA, PISA, WPSA, PSA, volume, #rotor, donorHB, accptHB, glob, QPpolrz, QPlogPC16, QPlogPoct, QPlogPw, QPlogPo/w, logS, QPLogKhsa, QPlogBB, #metabol. (Table 4). All the calculated values for NV2445 were compared with the calculated values for PTC124.

Table 4. Predictive ADME-Tox comparison between PTC124 and NV2445

molecule	**#stars** (0-5)	**MW** (130-725)	**Dipole** (1.0-12.5)	**IP(eV)** (7.9-10.5)	**EA(eV)** (-0.9-1.7)	**SASA** (300-1000)	**FOSA** (0-750)	**FISA** (7.0-330)
NV2445	0	280.3	6.2	9.5	1.2	536.0	73.4	144.2
PTC124	1	284.2	1.9	9.7	1.3	520.1	0	154.6

molecule	**PISA** (0-450)	**WPSA** (0-175)	**PSA** (7-200)	**Volume** (500-2000)	**#rotor** (0-15)	**donorHB** (0-6)	**accptHB** (2-20)	**Glob** (0.75-0.95)
NV2445	318.4	0	82.5	903.0	1	1	4.5	0.84
PTC124	333.4	32.1	85.1	866.8	1	1	5	0.84

molecule	**QPpolrz** (13-70)	**QPlogPC16** (4-18)	**QPlogPoct** (8-35)	**QPlogPw** (4-45)	**QPlogPo/w** (-2.0-6.5)	**QPlogKhsa** (-1.5-1.5)	**QPlogBB** (-3.0-1.2)	**#metab** (1-8)
NV2445	32.38	10.01	15.28	9.83	2.898	0.01	-0.85	2
PTC124	31.08	9.63	14.80	10.47	2.6	-0.17	-0.86	0

MW, molecular weight; **IP**, PM3 calculated ionization potential (negative of HOMO energy); **EA**, PM3 calculated electron affinity (negative of LUMO energy); **SASA**, Total solvent accessible surface area (SASA) in square angstroms using a probe with a 1.4 Å radius; **FOSA**, Hydrophobic component of the SASA (saturated carbon and attached hydrogen); **FISA**, Hydrophilic component of the SASA (SASA on N, O, H on heteroatoms, carbonyl C); **PISA**, (carbon and attached hydrogen) component of the SASA; **WPSA**, Weakly polar component of the SASA (halogens, P, and S); **Volume**, Total solvent-accessible volume in cubic angstroms using a probe with a 1.4 Å radius; **#rotor**, number of rotatable bonds; **donorHB**, number of h-bond donor, **accptHB**, number of H-bond acceptor; **glob**, Globularity descriptor, $(4\pi r^2)/(SASA)$, where r is the radius of a sphere with a volume equal to the molecular volume; **QPpolrz**, Predicted polarizability in cubic angstroms, **QPlogPC16**, Predicted hexadecane/gas partition coefficient; **QPlogPoct**, Predicted octanol/gas partition coefficient; **QPlogPw**, Predicted water/gas partition coefficient; **QPlogPo/w,** Predicted octanol/water partition coefficient.; **QPlogKhsa**, Prediction of binding to human serum albumin; **QPlogBB,** Predicted brain/blood partition coefficient; **#metab,** Number of likely metabolic reactions.

Furthermore, NV2445 respects the Lipinski's rule of five, and it has a predicted human oral absorption >80%. CYPP450 sites of metabolism for isoform 2C9 were also calculated for NV2445, and reported in Figure 9. Combined results show as the tolyl ring could represents a good site of metabolism for NV2445.

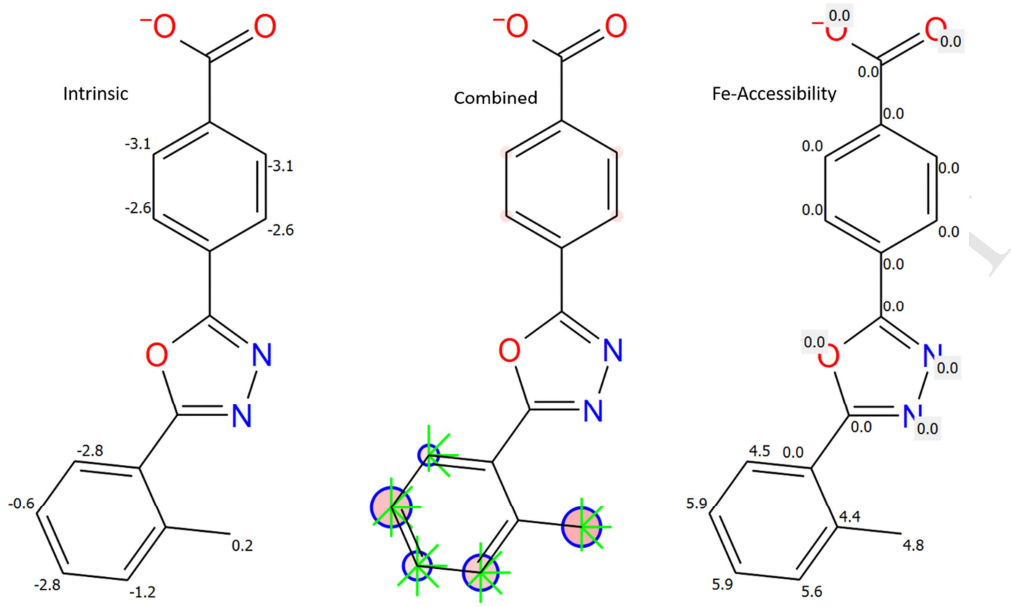

Figure 9. P450 site of metabolism (SOM). **Intrinsic reactivity**: positive values show high reactive site, negative values show weak reactive site; **Fe-accessibility**: positive values show high accessibility, negative values show poor accessibility, **Combined reactivity**: the number of rays indicates the values of the Fe-accessibility from IFD calculation, The circle encode 3 separate pieces of data.1) the size of the circles indicates the overall SOM score – the larger the circle the better the score, 2) the color of the circle indicates the atomic intrinsic reactivity – the redder the circle, the higher the intrinsic reactivity, 3) a blu ring around the circle indicates that the atom passed through the CYP filtering stage.

Detection of CFTR re-expression and localization on the cellular membrane of IB3.1 (CFTR ΔF508/W1282X) cells after treatment with PTC124 analogues. To evaluate if NV2445, besides allowing the readthrough of PTCs, was able to restore CFTR proper localization to the plasma membranes, a biological test involving a human IB3.1 cell line has been performed.

The IB3.1 is an immortalized human cell line from FC patient harboring two mutant alleles of CFTR (ΔF508 and W1282X) causing impaired plasma membrane normal localization. The CFTR protein was detected in cells not permeabilized by a specific antibody targeting its first

external portion. The IB3.1cells were treated with G418 (430 μM), PTC124 and NV2445 (both at 12 μM). Immunofluorescence microscopy images show that after a 24 hours treatment CFTR actually localize at the cell membrane suggesting the translation readthrough occurrence, CFBE41o-cells transfected with a CFTR WT construct was used as positive control of the CFTR expression (Figure 10A-B).

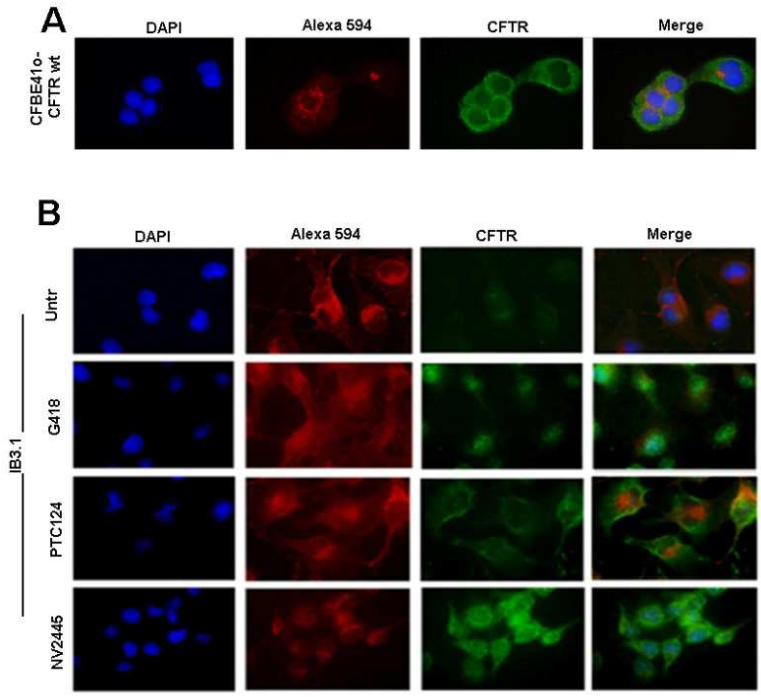

Figure 10. Immunofluorescence shows expression of the CFTR protein following the readthrough of the UGA stop codon in CFTR of IB3.1 human cells. **A)** Expression of CFTR in CFBE41o- (CFTRwt; positive control) cells and in **B) IB3.1 cells** untreated (untr; negative control), treated with G418 (positive control), with PTC124 and NV2445 for 24 hours. CFTR protein was revealed by a specific antibody targeting its first external loop (green, Alexa-488). Nuclei (blue) were DAPI stained. The cell membrane and Golgi apparatus were stained in red (WGA-Alexa 594).

To quantify the CFTR protein level after exposure to NV2445 we treated IB3.1 cells with PTC124 and NV2445 for 24 hours and extracted and purified the membrane protein fractions that were analyzed by western blot (Figure 11A-B). For the Western blot, we used a CFTR C-

terminal specific antibody. The treatment with the newly synthesized molecule NV2445 dramatically increased the presence of the CFTR protein in IB3.1 cell membrane fraction when compared to untreated (figure 11A-B).

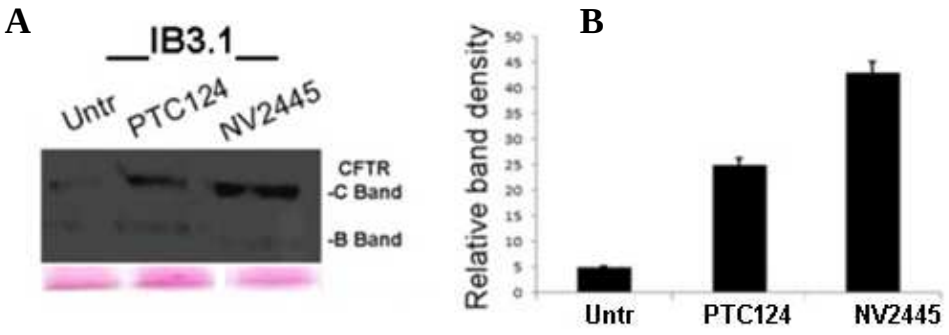

Figure 11. A) Western blot showing CFTR protein levels in membrane extracts of IB3.1 cells untreated (lane: 1) or treated with the indicated compounds (lane 2: PTC124; lane 3: NV2445). Ponceau red was used as a loading control. **B)** Histogram of the densitometry of the Western blotting bands. A primary antibody raised against the C-terminus of CFTR was used.

A successive step was to measure the efficacy of the readthrough activity of NV2445 in a primary human bronchial epithelial cell line (genotype: L1077P/W1282X) from CF patients, the results (SM section 1 and Figure S1) confirmed the results we observed in IB3.1 cells.

Treatment of the IB3.1 cells with NV2445 induces a functional CFTR protein. To ascertain the functionality of the re-expressed CFTR protein, produced after exposure to NV2445, a quench-EYFP assay was performed. This assay is based on iodide-mediated quenching rates of an ectopically expressed mutant form of the Yellow fluorescent protein (YFP). To this aim, IB3.1 and CFBE41o- cells were transfected with the plasmid pCDNA3.1 EYFP (M148Q; I152L) and selected for the resistance to the G418 antibiotic. Figure 12 shows the results of the EYFP

assay done in IB3.1 cells after 24 hours of exposition to PTC124 and NV2445. Cells were plated in a 6 well plate one day before the experiment, they were stimulated with forskolin (20 μM) for 20 min and placed in a buffer containing iodide (PBS1x similar buffer, NaCl is replaced by equimolars of NaI). Changes in fluorescence intensity were monitored by a Zeiss fluorescence microscope and the images were recorded every 1.5 s with a CCD digital camera (AxioCam, Zeiss).

Upon replacement of chloride for iodide we observed a rapid decline in EYFP fluorescence (Figure 12) in the IB3.1 cells treated with NV2445 and in positive control cells (PTC124; G418 treated cells).

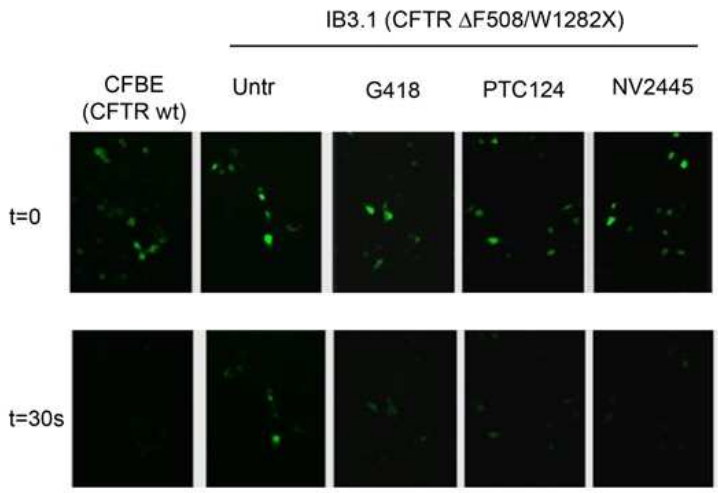

Figure 12. Exposure of IB3.1 cells to NV2445 induces functional expression of the CFTR protein channel. EYFP assay in CFBE41o- and IB3.1 cells transfected with the pcDNA3 YFP-H148Q-I152L vector, untreated or treated with the indicated compounds for 24 hour (G418: 430 μM; PTC124 and NV2445: 12 μM).

Despite the good results obtained on IB3 cells, during the YFP assay the long exposition to PBS/forskolin induced the detachment of many of them from the plate, reducing the number of analyzable cells. Moreover, the genotype of IB3 cells was not a homozygous for the stop

mutation, precisely the IB3.1 cells used in our experiment showed a CFTR allele with the ΔF508 mutation. Therefore, to confirm results observed with IB3.1 cells, we shifted to another cell line. To this aim we generated Fisher rat thyroid cell harboring the mutated (G542X) CFTR obtained by Site directed mutagenesis (see SM, Section 2, Figures S2, S3 and S4 for detailed information).

Production of FRT cells expressing nonsense-CFTR (nsCFTR) and evaluation of the CFTR expression after treatment with NV2445. To further evaluate the efficacy of NV2445 FRT cells were transfected with the pTracer vectors containing either the WT-CFTR ($CFTR^{WT}$) or the G542X-CFTR ($ns CFTR^{(G542X\text{-}opal)}$) human cDNA and selected by Zeocin resistance. The advantage of the use of these cells is that they do not express cAMP dependent channels (as CFTR) or CFTR protein. The expression of the $CFTR^{WT}$ and $ns CFTR^{(G542X\text{-}opal)}$ in transfected FRT cells was evaluated by qRT-PCR and Western blot (Figure 13).

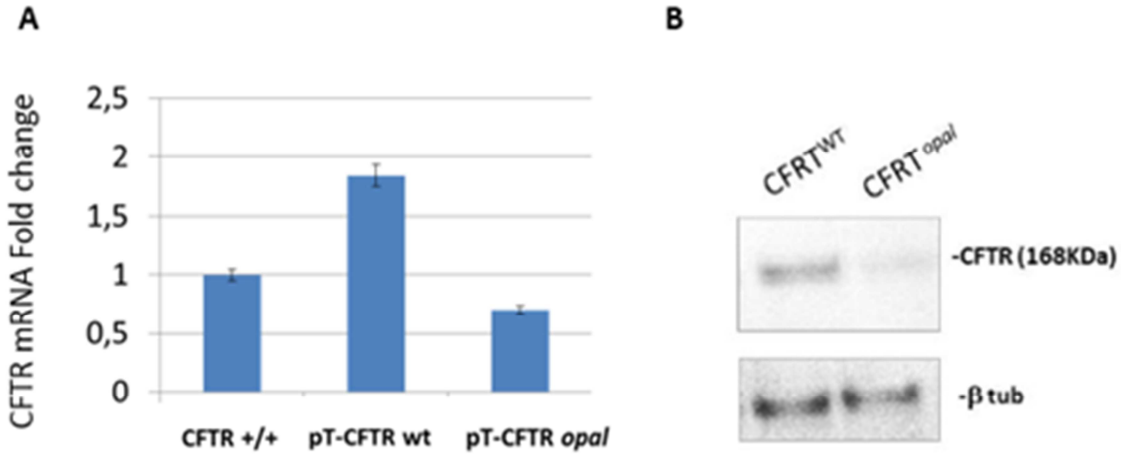

Figure 13. A) qRT-PCR to detect CFTR transcript expression after Zeocin selection in FRT cells. **B)** Western blot to detect CFTR protein in FRT transfected cells ($CFTR^{WT}$ and $ns CFTR^{(G542X\text{-}opal)}$). β-tubulin was used as control for protein loading.

The FRT cells were then treated with NV2445 (12 μM), PTC124 (12 μM) and G418 (430 μM) (as positive controls) for 24 hours and the expression of the human $CFTR^{WT}$ and *ns*$CFTR^{(G542X\text{-}opal)}$ was evaluated by immunofluorescence and Western blot analyses (Figure 14 A-C). Immunofluorescence microscopy images allow to visualize CFTR localization at the cell membrane suggesting the occurrence of translation readthrough and proper localization also in this cell type after NV2445 exposure (Figure 14 A). Similar results were obtained by the Western blot analysis. After 24 hours of treatment with NV2445 CFTR protein levels appreciably increase when compared with controls (Untreated and PTC124) (Figure 14 B-C).

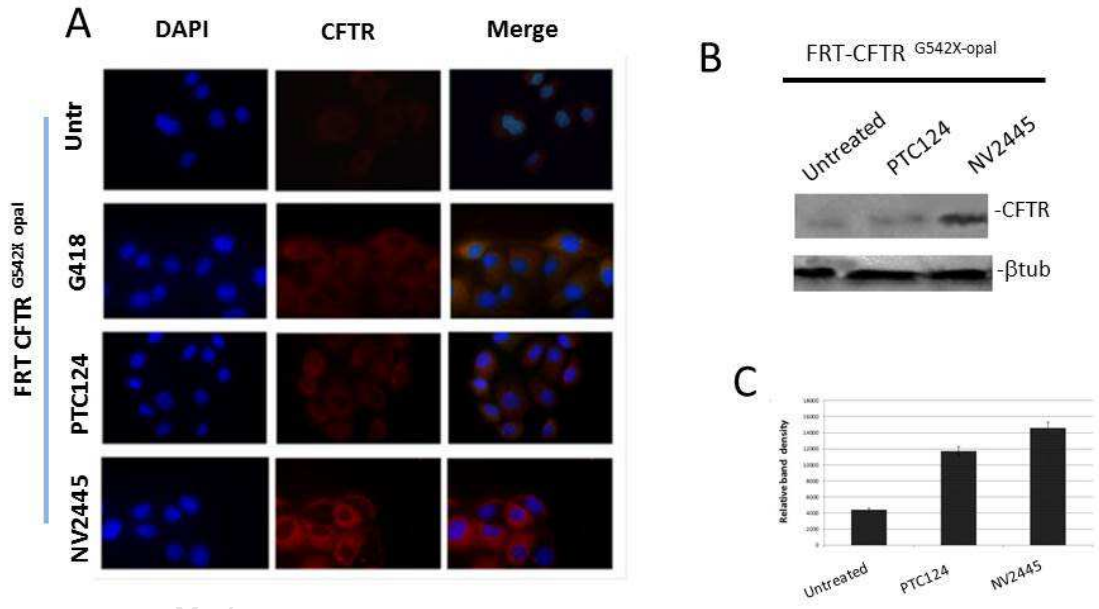

Figure 14. A) Immunofluorescence analysis to detect the CFTR protein following the readthrough of the UGA stop codon in $nsCFTR^{(opal)}$ FRT cells untreated (untr), treated with G418 (positive control) and with PTC124 and NV2445 for 24 h. CFTR protein was revealed by a specific antibody targeting its first external portion and a secondary antibody (SC2092-red). Nuclei (blue) were DAPI stained. **B)** Western blot analysis to detect CFTR protein in transfected FRT cells (FRT-$CFTR^{(gG542X\text{-}opal)}$) left untreated and treated with PTC124 and NV2445 for 24 h

β-tubulin was used as control for the protein loading. **C)** Quantization of the gel bands by ImageJ software.

Molecular and functional analyses by record in vitro of the transepithelial CFTR-mediated Cl- current and EYFP assay after NV2445 exposure indicated functional CFTR channel production in FRT cells. Our results showed that the exposition of *ns*CFTR$^{(opal)}$ FRT cells to the NV2445 induced the CFTR full-lenght protein expression and its membrane localization. Therefore, the next step was to analyse the functionality of the CFTR channel in our cell model system by two different approaches.

The first approach was to detect CFTR activity by the EYFP quenching assay. FRT cells ectopically expressing the EYFP protein, were used to perform the "halide sensor fluorescent assay". To evaluate CFTR activity/functionality, FRT EYFP cells (CFTR^{WT} and *ns*CFTR$^{(opal)}$) were treated with NV2445 and then analysed by fluorescent microscopy and fluorimetric assays (Figure 15 A-B).

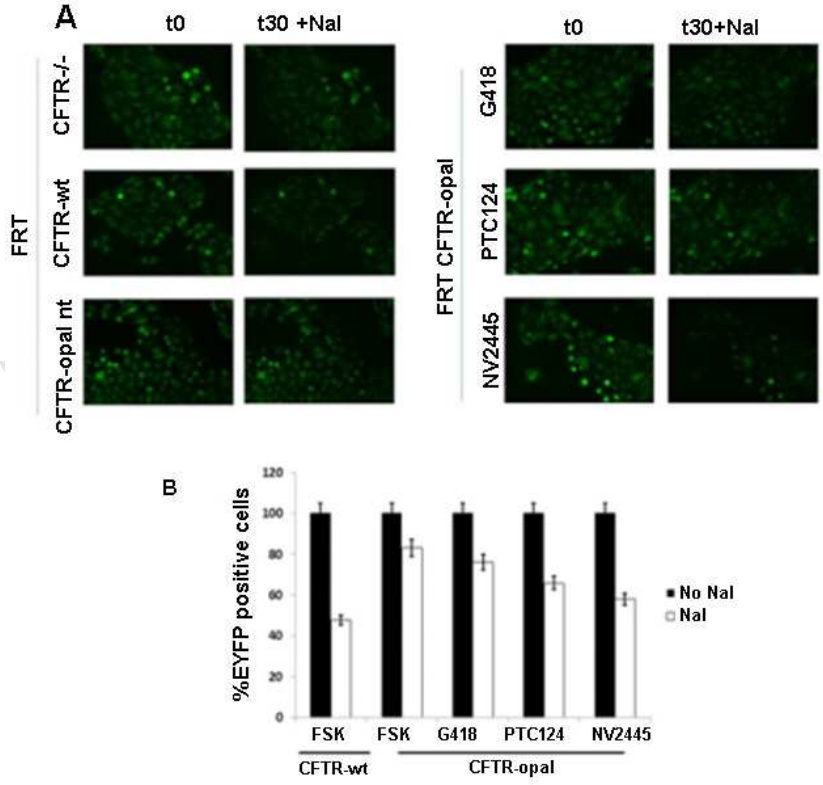

Figure 15. A) EYFP assay in FRT EYFP-CFTR^{WT} and CFTR^{opal} cells, untreated or treated with G418 (430 µM), PTC124 (12 µM) and NV2445 (12 µM) for 24 hours, pre-stimulated with forskolin (20 µM) for 20 min, before and post addition of NaI 137 mM to quench the EYFP fluorescence in presence of a functional CFTR channel. **B)** FRT EYFP-CFTR opal cells, untreated (only forskolin 20 µM for 20 min) or treated with G418 (430 µM), PTC124 (12 µM) and NV2445 (12 µM) for 24 hours, stimulated by forskolin 20 min before of the assay (with or without NaI addition).

By the second approach we measured the activity of the CFTR channel by using FRT cells that are able to differentiate in a tight epithelium thus allowing evaluation of CFTR channel functionality by trans-epithelial CFTR-mediated Cl^- current.

Cells were plated on Snapwell permeable supports for one week (sufficient time to induce epithelium formation) and then exposed to NV2445 and PTC124 for 24 hours (apical and basal). CFTR^{WT} FRT cells were used as positive controls while untreated *ns*CFTR $^{(G542X\text{-}opal)}$ *FRT* cells as negative controls.

In order to determine restoration of CFTR channel function, transepithelial CFTR-mediated Cl^- currents across cell monolayer was measured by Ussing Chamber. Under basal condition, there was no significantly difference in basal *Isc* among the samples (Figure 16). In CFTR^{WT} FRT epithelium, stimulation of monolayers with the adenylate cyclase activator FSK (20 µM) increased basal *Isc* by 27.5 µA/cm^2. Application of FSK in *ns*CFTR $^{(opal)}$ *FRT* treated with NV2445 and PTC124 produced a substantial increase in basal CFTR-dependent *Isc* by 17 µA/cm^2 and 11 µA/cm^2 respectively, whereas untreated *ns*CFTR $^{(G542X\text{-}opal)}$ *FRT* cells did not produce any increase in forskolin-stimulated chloride currents (Figure 16).

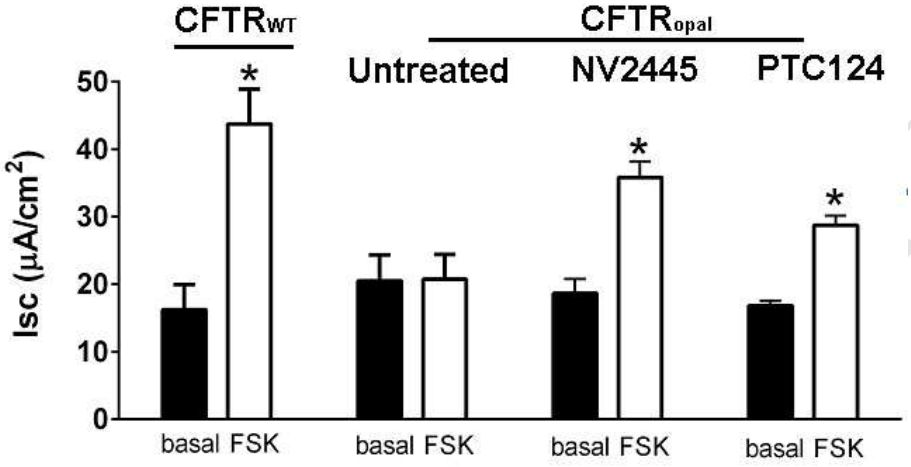

Figure 16. Characterization of CFTR-dependent Isc in nsCFTR $^{(G542Xopal)}$ FRT epithelium. Average of the basal current and of transepithelial CFTR-mediated Cl^- currents after application of FSK (20 μM) in WT-CFTR-FRT (positive control) and in nsCFTR $^{(opal)}$ FRT epithelium untreated or treated for 24 hours with PTC124 (12 μM) and NV2445 (12 μM).

In vitro analysis of the safety profile of NV2445. Primary human fibroblasts IMR90 were used to determine the possible cytotoxic effects of NV2445 and the impact on cell proliferation. In figure 17A-B are reported the percentages of dead cells and proliferating cells after treatment with 12 μM NV2445, 12 μM PTC124 and 430 μM G418. Our results showed that NV2445 and PTC124 induce an increase in dead cells at 24h (PTC124:30%; NV2445: 18%) and 72h (PTC124: 30%; NV2445: 21%) that was constant in the time. In contrast the G418 induced the 35% of dead cells at 24 hours and this percentage increased at 72 hours (51%). We observed that IMR90 cells proliferate as untreated cells when treated daily (every 24h) for 10 days with NV2445 (figure 17 C).

Similar results were observed by MTT assay performed nsCFTR $^{(G542X- opal)}$ FRT cells to evaluate the effects on cell viability at three different concentrations (12, 24, 48 μM) of the NV2445 after 24 and 72 hours of treatment (See SM Section 3 Figure S5).

The possible genotoxic effect of NV2445 was evaluated by comparing the expression of a DNA damage marker (γH2AX) after treatment with NV2445, PTC124 and Doxorubicin (DNA damage agent used by us as positive control). By immunofluorescence analysis using a primary antibody against γH2AX phosphorylated in Ser139 we detected γH2AX positive cells only in doxorubicin treated IMR90 (Figure 17 D).

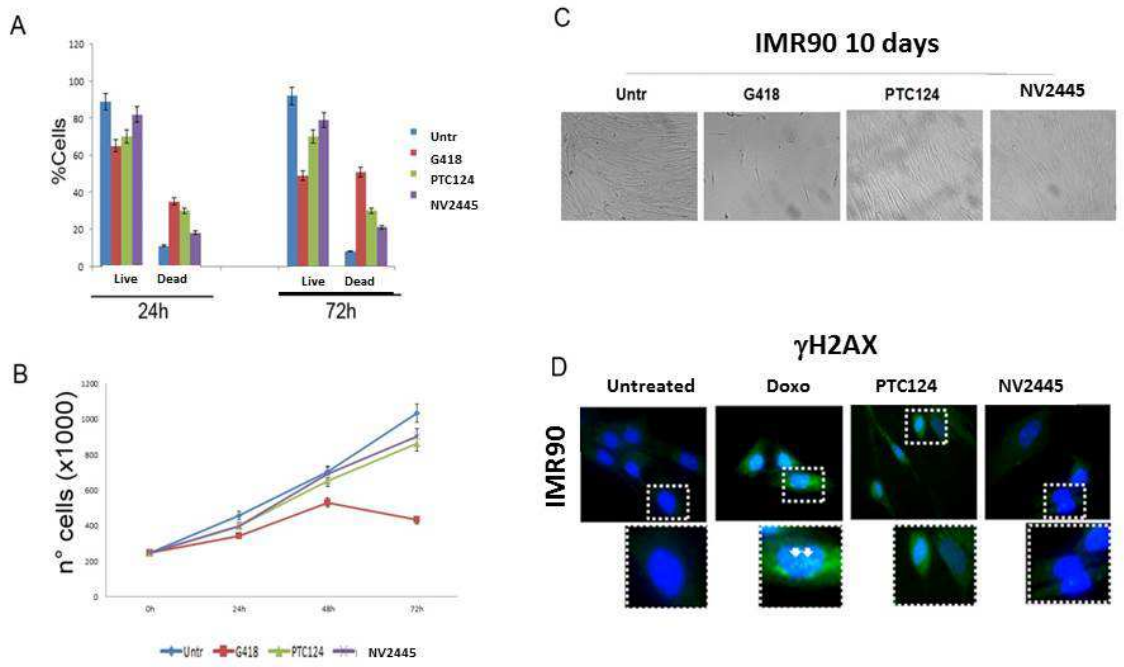

Figure 17. A) Percentages of live and dead IMR90 cells untreated or treated with G418 (430 μM), PTC124 (12 μM) and NV2445 (12 μM) for 24-72hours; and in **B)** the relative count of cell proliferation at the indicated time. **C)** Representative images of the primary human fibroblasts IMR90 after ten days of daily treatment (every 24h) with the indicated drugs. **D)** Evaluation of DNA damage (genotoxic effect) in IMR90 cells untreated or treated with Doxorubicin (430 μM), PTC124 (12 μM) and NV2445 (12 μM) for 72hours (Doxorubicin 0,2 μg/ml was used as positive control).

This result was confirmed by another analysis performed to identify a form of p53 phosphorylated in Ser15, specific for DNA damage response.

The results of the immunofluorescence analysis, reported in Figure 18, showed an increase of the Ser15 phosphorylated form of p53 in doxorubicin treated fibroblasts at 24 and 72 hours (with arrows). No signal in the nucleus was detected in PTC124 and NV2445 treated cells (Figure 18 A-B).

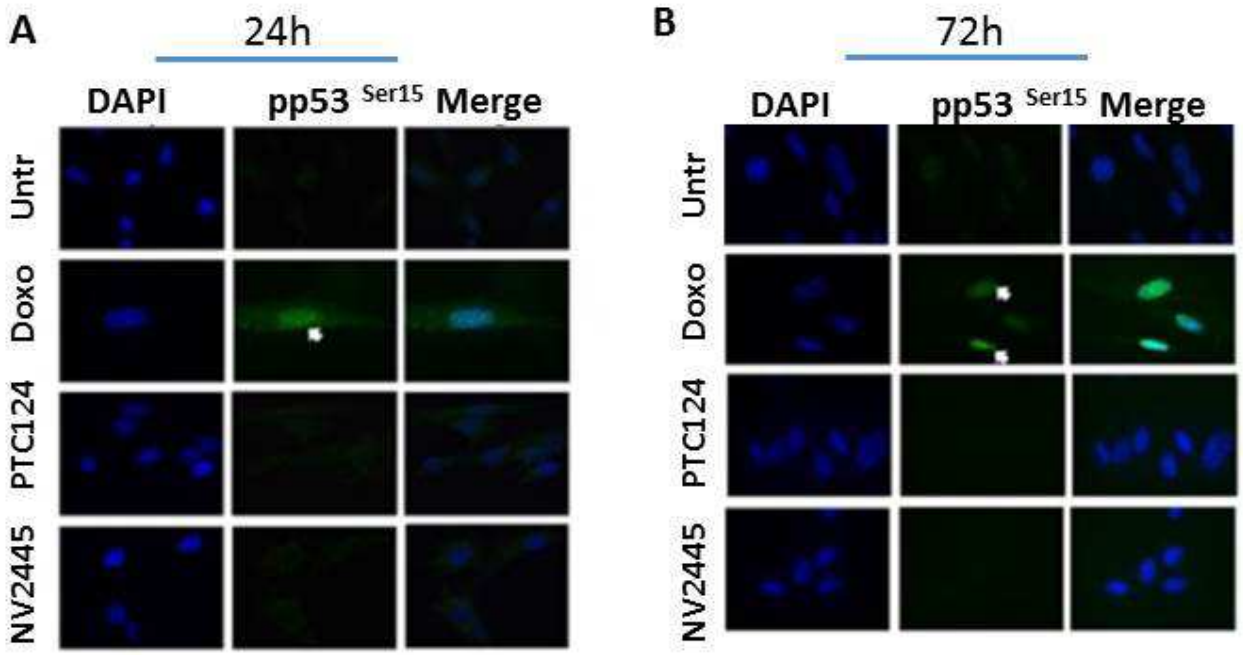

Figure 18. Immunofluorescence analysis to detect pp53 phosphorylated in Ser15 in IMR90 untreated or treated cells with Doxorubicin (0,2. μg/ml), PTC124 (12 μM) and NV2445 (12 μM) for 24 hours **(A)** and 72 hours **(B)**.

CONCLUSIONS.

In this work we identified, by computational screening, synthesis and biological analyses, a new small molecule with 1,3,4-oxadiazole core **NV2445** showing a high readthrough activity. We compared the activity of PTC124 with analogues differing in the heteroatoms position in the central heterocyclic core and found an interesting lead, NV2445, based on a 1,3,4-oxadiazole

scaffold with high potency as TRID. This was confirmed by the observation of the protein localization after readthrough on the cell membrane and its correct functionality after NV2445 treatment in CF model systems and in cells expressing a *nonsense*-CFTR-mRNA. Furthermore, we compared the predicted ADME properties of NV2445 and PTC124 demonstrating the better pharmacological properties of NV2445.

We studied the supramolecular interactions among TRIDs and CFTR-mRNA to assess the biological target/mechanism and in our hypothesis NV2445 as well as PTC124 interact with the premature termination codon and its surroundings in the mRNA encoding frame.

The fact that the efficacy of PTC124 in CF is still debated highlights the importance of further studies aiming to understand the readthrough mechanism and to find new readthrough agents.

Indeed, therapeutic nonsense suppression, besides respecting the principles of personalized medicine is to be considered a wide therapeutic approach since a single drug, focused on a specific genetic defect, may be beneficial to different diseases whose common denominator is a nonsense mutation.

EXPERIMENTAL SECTION.

Materials and Methods

3D-QSAR pharmacophore modeling. Concerning the 3D-QSAR pharmacophore modelling, processing procedures for the structures and models generation were obtained from previous papers [17, 22-27], using the Phase software [28, 29]. Models generated were measured according appropriate measures of goodness-of-fit, robustness, and predictive capability.

Used statistics for goodness-of fit are: R2, SD (standard deviation), F (Fisher test), RMSE (root mean square error), Pearson-R. Used statistics to measure robustness of the model are: Q^2(eq.1).

Eq.1 $$q^2 = 1 - \frac{\sum_{i=1}^{training}(y_i - \hat{y}_i)^2}{\sum_{i=1}^{training}(y_i - \bar{y})^2}$$

Where $\mathbf{y_i}$ $\mathbf{\hat{y}_i}$ are the actual and predicted activities of the ith molecule, respectively, and $\bar{\mathbf{y}}$ is the average activity of all molecules.

Predictive capability of the models generated was assessed by means of the external validation of the test set. Used statistics for external validation are: Q^2_{ext} (eq.2), Golbraikh and Tropsha parameters R^2_0 e R'^2_0, and k and k', r^2_m metrics > 0.65 [30-32].

Eq.2 $$q^2_{ext} = 1 - \frac{\sum_{i=1}^{test}(y_i - \hat{y}_i)^2}{\sum_{i=1}^{test}(y_i - \overline{y_{tr}})^2}$$

Where $\mathbf{y_i}$ $\mathbf{\hat{y}_i}$ are the actual and predicted activities of the ith molecule, respectively, $\bar{\mathbf{y}}_{\mathbf{tr}}$ is the average activity of all molecules in the training set

Chemistry. All solvents and reagents were obtained from commercial sources. All synthesized compounds were purified by silica flash chromatography and analyzed by IR, NMR and GC-MS or HPLC/MS to assess their structure and purity. In all the cases purity was higher than 95%. Melting points have been determined on a Kofler apparatus and are uncorrected. ^{1}H NMR and ^{13}C NMR spectra for all compounds were recorded on a 300 MHz spectrometer (Bruker 300 Avance), by using TMS as an internal standard and are reported in SM section 4. IR spectra were registered with a Shimadzu FTIR-8300 instrument. Chromatography was performed by using flash silica gel (Merck, 0.040-0.063 mm) and mixtures of ethyl acetate and petroleum ether

(fraction boiling in the range of 40-60 °C) in various ratios as eluents. GC-MS determinations were carried out on a Shimadzu GCMS-QP2010 system. HRMS spectra were recorded by analyzing a 10 ppm solution of the compound in a 6540 UHD Accurate-Mass Q-TOF LC/MS (Agilent Technologies) equipped with a Dual AJS ESI source, and are reported in SM section 5.

General procedure for the synthesis of 1,3,4-oxadiazoles. 0.01 mol of respective acid with hydrazine (0.012 mol), have been placed in a quartz tube in the absence of solvents and subjected to microwave irradiation at 900 W for 3 minutes. The obtained solid was left in the freezer for 2 hours and then freeze-dried in order to remove the water.

The solid was crystallized by methanol and further reacted with the opportune aldehyde, in equimolar amount, in refluxing ethanol.

The solvent was removed and then the solid was dissolved in DMSO (5 mL) and K_2CO_3 (1.2 equivalents) and I_2 (3 equivalents) were added. The reaction was allowed to stir at 100 °C for 2 hours. DMSO and Water were removed by freeze dryer and the 1,3,4-Oxadiazoles were obtained and further purified by chromatography and crystallization.

Oxadiazoles with an ester functionality were further subjected to hydrolysis: 0.01 mol of the respective methyl ester was dissolved in THF (5 mL) and 0.5mL of LiOH 10 M were added. The reaction was allowed to stir at room temperature overnight. The solvent was removed under vacuum, the solid was added with acidic water, after extraction with ethyl acetate the organic residue was further purified by crystallization.

NV2347 - methyl 4-(5-o-tolyl-1,3,4-oxadiazol-2-yl)benzoate. Yield 72%. White solid, m.p. 136-138°C from Ethanol. ^{1}H NMR (300MHz, $CDCl_3$): δ (ppm) 8.20 (m, 4H9, 8.05 (br d, 1H, J 7.7Hz), 7.45 (br t, 1H, J 7.7 Hz), 7.38 (br d, 1H, J 7.7 Hz), 7,36 (br t, 1H, J 7.7 Hz), 3.97 (s, 3H),

2.78 (s, 3H). ^{13}C (75 MHz, $CDCl_3$): δ (ppm) 166.3, 165.5, 163.5, 138.7, 132.9, 132.0, 131.6, 130.4, 129.2, 127.9, 127.0, 126.4, 122.8, 52.6, 22.3. IR (ν cm^{-1}) 1720. HRMS (ESI): Calcd. for $C_{17}H_{14}N_2O_3$ $(M+H)^+$ 295.1077, found 295.1071.

NV2653 - methyl 3-(5-(2-fluorophenyl)-1,3,4-oxadiazol-2-yl)benzoate. Yield 70%. White solid, m.p. 118-120 °C from Petroleum. ^{1}H NMR (300 MHz, $CDCl_3$): δ (ppm) 8.82 (s, 1H), 8.40 (d, 1H, J 9Hz), 8,25 (m, 2H), 7.70-7.59 (m, 2H), 7.36(m, 2H) 4.01 (s, 3H). ^{13}C (75 MHz, $CDCl_3$): δ (ppm) 166.1, 164.2 (d, J 1.2 Hz), 161.8 (d, J 5 Hz), 160.1 (d, J 258 Hz), 133.8 (d, J 8.4 Hz), 132.8, 131.4, 131.2, m129.9 (d, J 1.7 Hz), 129.5, 128.1, 124.8 (d, J 3Hz), 124.3, 117.1 (d, J 21 Hz), 112.3 (d, J 12 Hz), 52.6. IR (ν cm^{-1}) 1720. HRMS (ESI): Calcd. for $C_{16}H_{11}N_2O_3F$ $(M+H)^+$ 299.0826, found 299.0835.

NV924 - 5-methyl-1,3,4-oxadiazol-2-amine. Yield 80%. White solid, m.p. 176-180 °C from Ethanol. ^{1}H NMR (300 MHz, DMSO-d6): δ (ppm) 6.81 (br s, 2H, NH_2), 2.26 (3H, CH_3). ^{13}C (75 MHz, DMSO-d6): δ (ppm) 163.6, 156.2, 10.47. IR (nujol) (ν cm^{-1}) 3268, 3085. HRMS (ESI): Calcd. for $C_3H_5N_3O$ $(M+H)^+$ 100.0505, found 100.0512.

NV1191 - 2-(4-fluorophenyl)-5-phenyl-1,3,4-oxadiazole Yield 70%. White solid 148-149 °C from Petroleum; ^{1}H NMR (300 MHz, $CDCl_3$): δ (ppm) 8.20-8.09 (m, 4H), 7.58-7.66 (m, 3H), 7.49-7.42 (m, 2H). ^{13}C (75 MHz, DMSO-d6): δ (ppm) 164.2 (d, J 250 Hz), 164.1, 163.3, 132.1, 129.4 (d J 9 Hz), 129.4 (overlapped 2C), 126.7 (overlapped 2C), 123.3, 120.0, (d, J 3 Hz), 116.7 (d, overlapped 2C, J 22Hz). GC-MS : M^+ 240 (78), 183 (80), 121 (90), 103 (100), 95 (68), 77 (80). HRMS (ESI): Calcd. for $C_{14}H_9FN_2NaO$ $(M+Na)^+$ 263.0591, found 263.0597.

NV2712 - methyl 3-(5-(2,4,5-trifluorophenyl)-1,3,4-oxadiazol-2-yl)benzoate Yield 78%. White solid 136-138 °C from Ethanol ^{1}H NMR (300 MHz, $CDCl_3$): δ (ppm) 8.76 (t, 1H, J 1.6 Hz), 8.34 (dt, 1H, J 1.6 and 7.8 Hz), 8.24 (dt, 1H, J 1.6 and 7.8 Hz), 8.03 (m, 1H), 7.65 (t, 1H, J

7.8 Hz), 7.18 (m, 1H), 3.99 (s, 3H). IR (nujol) (ν cm^{-1}): 1750. HRMS (ESI): Calcd. for $C_{16}H_9N_2O_3F_3$ $(M+H)^+$ 335.0638, found 335.0651.

NV2445 - 4-(5-(*o*-tolyl)-1,3,4-oxadiazol-2-yl)benzoic acid. Yield 95%. White solid, m.p. 285-287°C from Ethanol. ^1H NMR (300 MHz, DMSO-d6): δ (ppm) 8.21 (d, 2H, J 8.2 Hz), 8.14 (d, 2H, J 8.2 Hz), 8.07 (br d, 1H, J 7.8 Hz), 7.55-7.41 (m, 3H), 2.68 (s, 3H). ^{13}C (75 MHz, DMSO-d6): 166.6, 164.7, 163.0, 137.9, 133.6, 131.8, 131.7, 130.3 (overlapped 2C),129.0, 127.0, 126.9 (overlapped 2C), 126.5, 122.3, 21.6. IR (ν cm^{-1}) 3500, 1700. HRMS (ESI): Calcd. for $C_{16}H_{12}N_2O_3$ $(M+H)^+$ 281.0921, found 281.0917.

NV2702 - 3-(5-(2-fluorophenyl)-1,3,4-oxadiazol-2-yl)benzoic acid. Yield 90%. White solid, m.p. 208-210°C from Ethanol. ^1H NMR (300 MHz, DMSO-d6): δ (ppm) 8.51 (br s, 1H), 8.25 (br d, 1H, J 7.8 Hz), 8.15-8.08 (m, 2H), 7.74-7.63 (m, 2H), 7.48-7.38 (m, 2H). ^{13}C (75 MHz, DMSO-d6): 166.4, 163.5 (d, J 1.2 Hz), 160.9 (d, J 5Hz), 159.3 (d, J 256 Hz), 134.3 (d, J 8.5 Hz), 132.5, 132.0, 130.6, 130.0, 129.7, 127.2, 123.3 (d, J 3.6 Hz), 123.6, 117.1 (d, J 21 Hz), 111.6 (d, J 11.5 Hz). IR (ν cm^{-1}) 3400, 1710. HRMS (ESI): Calcd. for $C_{15}H_9N_2O_3F$ $(M+H)^+$ 285.0669, found 285.0675.

NV2729 - 3-(5-(2,4,5-trifluorophenyl)-1,3,4-oxadiazol-2-yl)benzoic acid. Yield 93%. White solid, m.p. 232-234°C from Ethanol. ^1H NMR (300 MHz, DMSO-d6): δ (ppm) 8.62 (br s, 1H), 8.37 (m, 2H), 8.20 (br d, 1H, J 7.7 Hz), 7.95 (m, 1H), 7.78 (t, 1H, J 7.7 Hz). IR (ν cm^{-1}) 3480, 1710. HRMS (ESI): Calcd. for $C_{15}H_7N_2O_3F_3$ $(M+H)^+$ 321.0481, found 321.0489.

Cell culture conditions and transfection of reporter plasmid. HeLa and IB3.1 cells were cultured in DMEM supplemented with FBS 10% (GIBCO) in a humidified atmosphere of 5% CO_2 in air at 37°C.

Fisher rat thyroid (FRT) cells were cultured in Coon's modified F12 medium supplemented with 10% FBS, 2 mM glutamine, 2.68 g/L sodium bicarbonate, 100 U/mL penicillin and 100 µg/mL streptomycin (removed before of the readthrough experiments). Human primary broncoepithelial cells (BE-CFTR^{wt}; BE-CFTR$^{L1077P/W1282X}$) were provided by Italian cystic fibrosis foundation (*FFC-Service*). Be cells were cultured in LCH9/RPMI 1640 medium (1:1) (by *FFC-Service*). Cells were cultured in 75 cm^2 flasks coated with rat tail collagen for 2-4 passages. Cells were plated in snapwell (Corning 3801) supports and after 24 hours the medium was substituted with DMEM/F12, 2% Ultraser G (by *FFC-Service*). The medium was replaced every day, after 10 days was removed the apical medium to induce the differentiation and the cells were cultured in air/liquid state for 4 weeks.

Measurement of Luciferase activity by luminescence. HeLa cells plated in a 6 well plate at a density of 2x105/mL were transfected with WT (Fluc) andmutant (Fluc-opal) plasmids, by using lipofectamine 2000 (Invitrogen). Cells were incubated for 24 hours and PTC124 and the others compounds (12 µM) were added for additional 24 hours. Next, cells were washed with PBS, incubated with the detection mix Steady-Glo luciferase reagent (Promega) and 200 µL of cell suspension were plated in triplicate in a 96 well. Luciferase activity was measured on a luminometer (Promega).

Immunofluorescence Microscopy. To visualize H2BGFP expression cells were grown on rounded glass coverslips and fixed with methanol 100% for 2 min, permeabilized with 0.01% TritonX (Sigma-Aldrich) in PBS for 15 min and blocked with 0.1% BSA for 30 min, both at room temperature. Coverslips were incubated overnight at 4 °C with a mouse monoclonal antibody against GFP (Sigma-Aldrich, diluted 5 µg/mL) derived from mice immunized with a

synthetic peptide corresponding to amino acids 132−144 of the GFP from jellyfish Aequorea victoria, followed by a goat antimouse IgGFITC secondary antibody (Sigma-Aldrich, diluted 1:200) for 1 h at 37 °C. Nuclei were visualized with 1 μg/mL of 4′,6- diamidino-2-phenylindole (DAPI) and examined on a Zeiss Axioskop microscope equipped for fluorescence, images were captured with a CCD digital camera (AxioCam, Zeiss) and then transferred to Adobe PhotoShop for printing.

To visualize the CFTR protein, cells were grown on rounded glass coverslips and fixed with methanol for 2 min. The cell membrane and Golgi apparatus were stained by the Wheat Germ Agglutinin (WGA) Alexa 594 (Life Technologies). Coverslips were incubated with a mouse monoclonal antibody (CF3) that recognizes the first extracellular loop of human CFTR (Abcam, 1:500) overnight at 4 °C, followed by a goat polyclonal to mouse Alexa-Fluor-488 (Abcam, 1:1000) secondary antibody for 1 hour at 37 °C. Nuclei were visualized with DAPI. Cells were examined under a Zeiss Axioskop microscope equipped for fluorescence.

To detect p53 expression were used an anti-p53 (Ser15) antibody (rabbit, Santa Cruz 1:100) and FITC-conjugated anti-rabbit Santa Cruz, 1:200).

To evaluate DNA damage, the γH2AX (Ser139) state was detected by anti-γH2AX (Ser139) (Upstate, 1:100 in BSA 0.1%, rabbit) and by the secondary antibody anti-rabbit FITC (Santa Cruz; 1:100 in BSA 0,1%) at 37 °C for 1 hour. Nuclei were visualized with DAPI. Cells were examined under a Zeiss Axioskop microscope equipped for fluorescence.

Western Blotting. Proteins (50 μg) were separated by 10% SDS-PAGE and 4-12% SDS-PAGE containing 0.1% SDS and transferred to Hybond-C nitrocellulose membranes (Amersham Life Science) by electroblotting. The membrane was incubated with a goat polyclonal antibody anti–

CFTR (C-19, Santa Cruz 1:500) raised against a peptide mapping near the C-terminus of CFTR of human origin, and HRP-conjugated anti-goat (Abcam, 1:5000). The target protein was detected by ECL reagents (Pierce). We used β-tubulin antibody (mouse; Sigma-Aldrich 1:10.000) to confirm equal proteins loading. Gel bands were quantified by Image Lab software.

Real Time RT-PCR. Primers used in real-time RT-PCR experiments were designed with Primer Express software (Applied Biosystems, Monza, Italy) or based on Kerem et. al. [12]. Amplicons size was of approximately 70–100 bp. When not already tested the selected sequences were blasted against public databases using BLAST to confirm the identity of the genes. Total RNA was extracted from cells by using the RNAeasy Mini kit according to manufacturer's instruction (Qiagen, Milano, Italy). RNA was reverse-transcribed in a final volume of 50 µL using the High Capacity cDNA Archive kit (Applied Biosystems, Monza, Italy) for 10 min at 25 °C and 2 h at 37 °C. For each sample 2 µL of cDNA, corresponding to 100 ng of reverse transcribed RNA, was analyzed by real-time RT-PCR (95 °C for 15 sec., 60 °C for 60 sec repeated for 40 cycles), in quadruplicate, using the ABI PRISM 7300 instrument (Applied Biosystems, Monza, Italy). Real-time RT-PCR was done in a final volume of 20 µL comprising 1x Master Mix SYBR Green (Applied Biosystems, Monza, Italy) and 0.3 µM of forward and reverse primers for CFTR (Fwd: 5'-CTACATGGAACACATACCTTCG-3'; Rev: 5'-GGTGATAATCACTGCATAGC-3'), or GAPDH (Fwd:5′-CTCATGACCACAGTCCATGCC-3′; Rev: 5′-GCCAATCCACAGTCTTCTGGGT-3′). Data were analyzed by averaging quadruplicates Ct (cycle threshold). Levels of RNA were determined by using the SDS software version (Applied Biosystems, Monza, Italy) according to the $2^{-\Delta\Delta Ct}$ method and Ct values were normalized to the internal control GAPDH.

Microscope fluorescence YFP assay. FRT cells expressing the human WT-CFTR or G542X-CFTR cDNA together with the halide-sensitive YFP were plated in a 96 wells and after 24 hours the cells were treated with the test compounds for 24 hours. After 24 hours they were washed with Phosphate buffered saline (PBS: 137 mM NaCl, 2.7 mM KCl, 8.1 mM Na_2HPO_4, 1.5 mM KH_2PO_4, 1 mM $CaCl_2$, and 0.5 mM $MgCl_2$) and pre-stimulated for 20 min with forskolin (20 μM, acute dose) in a final volume of 60 μL in PBS1X. Microplates were then transferred to a fluorescence microscope (ZEISS, Germany) to detect YFP quenching induced by addition of NaI. Images were captured by Axiocam ZEISS at the t^0 and 30 seconds post addition of 165 μL of an iodide-containing solution (PBS-NaI). The final iodide concentration was 100 mM/well. The exposition time was 800 ms for all captured images.

Microplate reader fluorescence YFP assay. FRT cells expressing G542X-CFTR and the halide-sensitive YFP were plated in a 96 well and after 24 hours cells were treated with the test compounds for 24 hours. The third day the cells were washed with PBS1X (containing 137 mM NaCl, 2.7 mM KCl, 8.1 mM Na_2HPO_4, 1.5 mM KH_2PO_4, 1 mM $CaCl_2$, and 0.5 mM $MgCl_2$) and stimulated for 20 min with forskolin (20 μM) in a final volume of 60 μL. Microplates were then transferred to a microplate reader (GloMax®-Multi Detection System, Promega, Italy) for CFTR activity determination. Each assay consisted of a continuous 10 s fluorescence reading and 30 s after injection of 165 μL of an iodide-containing solution (PBS minus NaCl and plus NaI to replace Cl^- with I^-). Final iodide concentration in the wells was 100 mM.

Site direct mutagenesis. Site Directed Mutagenesis of the full-length CFTR cDNA was performed with the QuikChange® II Site-Directed kit (Stratagene). The plasmid harbouring CFTR cDNA was amplified with the following mutant primers: 5'-tgattccaccttctc**a**aagaactatattgtctttctctgcaaac-3' g1624tup (reverse) 5'-gtttgcagagaaagacaatatagttctt**t**gagaaggtggaatca-3' g1624tdw (forward).

Following user's manual, methylated parental template (isolated from dam+ E. coli) was removed by treatment with DpnI restriction enzyme (target: 5'Gm6ATC3´). Newly synthesized plasmids were transformed into XL1-Blue competent cells. "Colony PCR", which does not require DNA purification, was performed with two primers perfectly annealing to the template at 52 °C, CFTRup2 25'-ctaatgagaaacggtgtaag-3' (reverse) and CFTRdw1 5'-ggtgattatgggagaactgg-3' (forward). "Selective PCR" was performed with the forward selective primer g1624t 5'-gagaaagacaatatagttcttt-3' and the reverse primer CFTRup2 5'-ctaatgagaaacggtgtaag-3'. Reactions required a thermostable DNA polymerase lacking 3' to 5' proofreading activity (DyNAzyme™ II DNA Polymerase) and identical amount (10 ng) of purified plasmid DNA, either wt or mutagenized. To distinguish between mutant and wtDNA, a gradient thermocycler and primer annealing temperatures ranging from 44 to 52 °C were used. Positive controls (C+) were included where the same DNAs were amplified with the CFTRup2/CFTRdw1 primers (Ta 52 °C). Successful mutagenesis was finally confirmed by sequencing (BRM genomics; see SM Figure S4).

Short-circuit current measurements. Epithelial cell lines were grown on 1.12 cm^2 snapwell inserts. The filters were mounted between halves of Ussing flux chambers. It was bathed on both sides, with 10 mL of oxygenated (95% O_2 and 5% CO_2) Krebs solution, maintained at 37 °C by

circulation from a temperature-controlled water bath. The basolateral solution contained (in mM): 119 NaCl, 4.5 KCl, 2.5 $MgSO_4$, 25 $NaHCO_3$, 1.2 KH_2PO_4, 2.5 $CaCl_2$, 11.1 glucose. In the apical solution, 60 mM NaCl was replaced by Na gluconate. Short-circuit current (*Isc*) was measured as described previously [33, 34]. The cultures were voltage-clamped at 0 mV by using a voltage-clamp apparatus (EVC-4000; World Precision Instruments, Sarasota, FL). After 30 minutes stabilization period, forskolin (FSK) (20 µM, both sides) were added, while *Isc* was continuously recorded. The short-circuit current differences between baseline and plateau of stimulation was measured and compared between ns-CFTR, wt-CFTR , NV2445- CFTR and PT124-CFTR FRT cells as an index of CFTR function.

Cell viability: MTT assay. Cell viability was assayed by using MTT Vybrant kit (Thermo Fisher Scientific, USA). Cells were seeded in a 96-well plate at a density of 10^4 cells/well in 200 µL of culture medium with only vehicle (PBS) or test compounds at different concentrations (12 µM, 24 µM, 48 µM) for 24 and 72 hours. FRT cells were incubated at 37 °C in a humidified incubator. Additionally, six wells were left empty for cell-free background reference. The medium was refreshed with a solution containing 100 µL of fresh medium and 10 µl of the 12 mM MTT stock solution in PBS to each well. The microplate was incubated for 4 h at 37 °C, 5% CO_2. The plate was centrifuged at 1000 rpm for 10 min and the medium totally removed from each well followed by the addition of 100 µL of DMSO to solubilize the MTT formazan. The absorbance of each well was measured at 570 nm on a multiplate reader (GloMax®-Multi Detection System, Promega, Italy). The percentage of viable cells was measured as follows: % viability=OD of treated cells/OD untreated (only vehicle) cells; OD: optical density. The assay was conducted in triplicate.

Induced Fit Docking and Molecular Dynamics simulations. IFD is a mixed MD/docking approach in which the receptor residues (in this case the mRNA) surrounding the ligand are allowed to adapt their conformations to the ligand. Also for this approach, processing procedures used were obtained from previous works [25,35] using the Induced Fit software [36-38]. The MD simulations were performed with DESMOND 4.2 using the OPLS3 force field [39-41]. The complexes were solvated in cubic boxes using the TIP3P water model. Ions were added to neutralize charges. The system was minimized and equilibrated at a temperature of 303.15 K and at 1.013 bar pressure. The system was simulated as NPT ensemble, a Nose-Hover thermostat and Martyna-Tobia-Klein barostat were used. The integration time step was chosen to be 2 fs. In order to keep the hydrogen - heavy atom bonds rigid, the SHAKE algorithm was utilised. A 9 Å cut-off radius was set for the short range Coulomb interactions and smooth particle mesh Ewald was used for the long range interactions.

MM-GBSA free energy calculations. This method combines molecular mechanics energy and implicit solvation models at a reasonable computational cost. We applied this method to snapshots extracted from the 100.0 ns production MD trajectories. Protein–ligand binding free energy using MM-GBSA was calculated as the difference between the energy of the bound complex and the energy of the unbound protein and ligand. The method allows free energy decomposition into contributions originating from different types of physical-chemical interactions. Specifically, the energy is calculated for the protein–ligand complex, the ligand, and the protein, and their energies were computed using the OPLS3 force field with the generalized Born implicit solvent model, in order to calculate the averaged binding free energy (ΔG).

The following equations were considered to calculate the binding free energy:

ΔGbind= ΔE + ΔGsolv + ΔGSA

ΔE = Ecomplex - Eprotein - Eligand

Where Ecomplex, Eprotein, and Eligand define the minimized energies of protein–inhibitor complex, protein, and inhibitor, respectively.

ΔGsolv = Gsolv (complex) - Gsolv (protein) -Gsolv (ligand)

Where Gsolv (complex), Gsolv (protein), and Gsolv (ligand) are the solvation free energies of protein–inhibitor complex, protein, and inhibitor, correspondingly.

ΔGSA = GSA (complex) - GSA (protein) - GSA (ligand)

Where GSA (complex), GSA (protein), and GSA (ligand) are the surface area energies for protein–inhibitor complex, protein and inhibitor, respectively.

the entropy term –TΔS was not calculated to reduce computational time.

ADME-TOX predictions. The QikProp program [42] was used to obtain the ADME properties of NV2445, and PTC124. It predicts both physically significant descriptors and pharmaceutically relevant features, such as principal descriptors and physiochemical properties. It also evaluated the drug-like acceptability of the compounds, based on Lipinski's rule of five, essential for rational drug design. CYP450 Site of metabolism were also calculated

Declarations of interest: none

ASSOCIATED CONTENT

Supplementary Material

The following file (PDF) is available free of charge including:

(1) Detection of CFTR re-expression in primary bronco-epithelial cells from FC patients with CFTR ΔF508/W1282X after treatment with PTC124 analogues

(2) Site directed mutagenesis: introduction of the G542X mutation in the full-lenght CFTR cDNA

(3) MTT assay

(4) ^{1}H and ^{13}C NMR spectra for all compounds

(5) HRMS spectra

AUTHOR INFORMATION

Corresponding Authors

* Tel: Ivana Pibiri +39-091-23897545; Laura Lentini +39-091-23897341

email: Ivana Pibiri, ivana.pibiri@unipa.it; Laura Lentini, laura.lentini@unipa.it.

Author Contributions

The manuscript was written through contributions of all authors. All authors have given approval to the final version of the manuscript. ‡These authors contributed equally.

ACKNOWLEDGMENT

This work has been financially supported by the Italian Cystic Fibrosis Research Foundation, grant FFC#1/2014 and FFC#3/2017 with the contribution of Delegazione di Palermo,

Delegazione di Vittoria (Ragusa) e Siracusa and Delegazione FFC di Catania Mascalucia to Laura Lentini and Ivana Pibiri.

We thank Prof. J. Inglese, NIH Chemical Genomics Center, National Institutes of Health, Bethesda, for providing us with the FLuc190UGA plasmid, Prof. Louis Galietta (TIGEM, Napoli, Italy) and Dott.ssa Loretta Ferrera (Gaslini Hospital, Genova, Italy) for kindly providing us the FRT cells and the pTracer CFTR-WT vector; Dott.ssa Paola Melotti (Azienda Ospedaliera Universitaria Integrata Verona, Italy) for kindly providing us the IB3.1 cells.

REFERENCES

(1) Rowe, S.M. ; Miller, S. ; Sorscher, E.J. Cystic fibrosis. *N. Engl. J. Med.* **2005**, *352*, 1992-2001

(2) Son, J.-H.; Zhu, J.S.; Phuan, P.-W.; Cil, O.;Teuthorn, A.P.; Ku, C.K.; Lee, S.; Verkman, A.S.; Kurth, M.J. High-Potency Phenylquinoxalinone Cystic Fibrosis Transmembrane Conductance Regulator (CFTR) Activators. *J. Med. Chem.*, **2017**, *60* , 2401-2410

(3) Ye, L.; Hu, B.; El-Badri, F.; Hudson, B.M.; Phuan, P.-W.; Verkman, A.S.; Tantillo, D.J.; Kurth, M.J. Δf508-CFTR correctors: Synthesis and evaluation of thiazole-tethered imidazolones, oxazoles, oxadiazoles, and thiadiazoles. *Bioorg. Med. Chem. Lett.*, **2014**, *24*, 5840-5844

(4) Coffman, K.C.; Nguyen, H.H.; Phuan, P.-W.; Hudson, B.M.; Yu, G.J.; Bagdasarian, A.L.; Montgomery, D.; Lodewyk, M.W.; Yang, B.; Yoo, C.L.; Verkman, A.S.;

Tantillo, D.J.; Kurth, M.J. Constrained bithiazoles: Small molecule correctors of defective δf508-CFTR protein trafficking. *J. Med. Chem.*, **2014**, 57, 6729-6738

(5) Ponzano, S.; Nigrelli, G.; Fregonese, L.; Eichler, I.; Bertozzi, F.; Bandiera, T.; Galietta, L. J.V.; Papaluca, M. A European regulatory perspective on cystic fibrosis: current treatments, trends in drug development and translational challenges for CFTR modulators. Eur. Resp. Rev., **2018**, *27*, 170124

(6) Liessi, N.; Cichero, E.; Pesce, E.; Arkel, M.; Salis, A.; Tomati, V.; Paccagnella, M.; Damonte, G.; Tasso, B.; Galietta, L.J.V.; Pedemonte, N.; Fossa, P.; Millo, E. Synthesis and biological evaluation of novel thiazole- VX-809 hybrid derivatives as F508del correctors by QSAR-based filtering tools. Eur. J. Med. Chem., **2018**, *144*, 179-200.

(7) Burke J.F.; Mogg A.E. Suppression of a nonsense mutation in mammalian cells *in vivo* by the aminoglycoside antibiotics G-418 and paromomycin. *Nucleic Acids Res.*, **1985**, *13*, 6265-6272

(8) Manuvakhova, M.; Keeling, K.; Bedwell, D.M. Aminoglycoside antibiotics mediate context-dependent suppression of termination codons in a mammalian translation system. *RNA*, **2000**, *6*, 1044-1055

(9) Prayle, A.; Smyth, A.R. Aminoglycoside use in cystic fibrosis: therapeutic strategies and toxicity. *Curr. Opin. Pulm. Med.* **2010**, *16*, 604-610

(10) Rowe, S.M.; Mutyam, V.; Alroy, I.; Huertas, P. Translational read-through of CFTR nonsense mutations and inducement of cystic fibrosis transmembrane conductance regulator (CFTR) function by ELX-02 treatment. *J. Cyst. Fibros.* **2018**, *17, S2*

(11) Welch, E.M.; Barton, E.R.; Zhuo, J.; Tomizawa, Y.; Friesen, W.J.; Trifillis, P.; Paushkin, S.; Patel, M.; Trotta, C.R.; Hwang, S.; Wilde, R.G.; Karp, G.; Takasugi, J.; Chen, G.; Jones, S.; Ren, H.; Moon, Y.C.; Corson, D.; Turpoff, A.A.; Campbell, J.A.; Conn, M.M.; Khan, A.; Almstead, N.G.; Hedrick, J.; Mollin, A.; Risher, N.; Weetall, M.; Yeh, S.; Branstrom, A.A.; Colacino, J.M.; Babiak, J.; Ju, W.D.; Hirawat, S.; Northcutt, V.J.; Miller, L.L.; Spatrick, P.; He, F.; Kawana, M.; Feng, H.; Jacobson, A.; Peltz, S.W.; Sweeney, H.L. PTC124 targets genetic disorders caused by nonsense mutations. *Nature* **2007**, *447*, 87-91

(12) Kerem, E.; Hirawat, S.; Armoni, S.; Yaakov, Y.; Shoseyov, D.; Cohen, M.; Nissim-Rafinia, M.; Blau, H.; Rivlin, J.; Aviram, M.; Elfring, G.L.; Northcutt, V.J.; Miller, L.L.; Kerem, B.; Wilschanski M. Effectiveness of PTC124 treatment of cystic fibrosis caused by nonsense mutations: a prospective phase II trial. *Lancet*, **2008**, *372*, 719-727

(13) Kerem, E. MD and Cystic Fibrosis Ataluren Study Group. A randomized placebo controlled trial of ataluren for the treatment of nonsense mutation cystic fibrosis. *Lancet Respir Med.* **2014**, *2*, 539-547

(14) Kerem, E.; Konstan, M.W.; De Boeck, K.; Accurso, F.J.; Sermet-Gaudelus, I.; Wilschanski, M.; Elborn, J.S.; Melotti, P.; Bronsveld, I.; Fajac, I.; Malfroot, A.; Rosenbluth, D.B.; Walker, P.A.; McColley, S.A.; Knoop, C.; Quattrucci, S.; Rietschel, E.; Zeitlin, P.L.; Barth, J.; Elfring, G.L.; Welch, E.M.; Branstrom, A.; Spiegel, R.J.; Peltz, S.W.; Ajayi, T.; Rowe, S.M. Ataluren for the treatment of nonsense mutation

cystic fibrosis: a rondomised double blind, placebo controlled phase 3 trial. *Lancet Respir Med* **2014**, *2*, 539-547

(15) Aslam, A.A.; Higgins, C.; Sinha, I.P.; Southern, K.W. Ataluren and similar compounds (specific therapies for premature termination codon class I mutations) for cystic fibrosis. *Paediatr Respir Rev.* **2017**, 24, 32-34

(16) Raymer, B.; Bhattacharya, S. K.; Lead-like Drugs: A Perspective. *J. Med. Chem.* ***2018****, in press,* DOI:10.1021/acs.jmedchem.8b00407

(17) Pibiri, I.; Lentini, L.; Melfi, R.; Gallucci, G.; Pace, A.; Spinello, A.; Barone, G.; Di Leonardo, A. Enhancement of premature stop codon readthrough in the CFTR gene by Ataluren (PTC124) derivatives. *Eur. J. Med. Chem.* **2015**; 101, 236-244

(18) Pibiri, I.; Lentini, L.; Tutone, M.; Melfi, R.; Pace, A.; Di Leonardo, A. Exploring the readthrough of nonsense mutations by non-acidic Ataluren analogues selected by ligand-based virtual screening. *Eur.J Med Chem*, **2016**, *122*, 429-435.

(19) Boström, J.; Hogner, A.; Llinaș, A.; Wellner, E.; Plowright, A.T. *J. Med. Chem.* **2012**, *55*, 1817−1830

(20) Auld, D.S.; Lovell, S.; Thorne, N.; Lea, W.A.; Maloney, D.J.; Shen, M.; Rai, G.; Battaile, K.P.; Thomas, C.J.; Simeonov, A.; Hanzlik, R.P.; Inglese, J. Molecular basis for the high-affinity binding and stabilization of firefly luciferase by PTC124. *Proc Natl Acad Sci USA.* **2010**, *107*, 4878-83

(21) Lentini, L.; Melfi, R.; Di Leonardo, A.; Spinello, A.; Barone, G.; Pace, A.; Palumbo Piccionello, A.; Pibiri, I. Towards a rationale for the PTC124 (Ataluren)

promoted read-through of premature stop codons: a computational approach and GFP-reporter cell-based assay. *Mol. Pharm.* **2014**, *11*, 653-664

(22) Roy, B.; Friesen, W.J.; Tomizawa, Y.; Leszyk, J.D.; Zhuo, J.; Johnson, B.; Dakka, J.; Trotta, C.R.; Xue, X.; Mutyam, V.; Keeling, K.M.; Mobley, J.A.; Rowe, S.M.; Bedwell, D.M.; Welch, E.M.; Jacobson A. Ataluren stimulates ribosomal selection of near-cognate tRNAs to promote nonsense suppression, *PNAS* **2016**, *113*, 12508-12513

(23) Almerico, A.M.; Tutone, M.; Lauria, A. 3D-QSAR pharmacophore modeling and in silico screening of new Bcl-xl inhibitors. Eur. J. Med. Chem. **2010**, *45*, 4774-4782

(24) Lauria, A.; Ippolito, M.; Fazzari, M.; Tutone, M.; Di Blasi, F.; Mingoia, F.; Almerico, A.M. IKK-β inhibitors: An analysis of drug-receptor interaction by using Molecular Docking and Pharmacophore 3D-QSAR approaches *J. Mol. Graph. Model.* **2010**, *29*, 72-81

(25) Almerico, A.M.; Tutone, M.; Lauria, A. Receptor-guided 3D-QSAR approach for the discovery of c-kit tyrosine kinase inhibitors *J. Mol. Model*. **2012**, *18*, 2885-2895.

(26) Almerico, A.M.; Tutone, M.; Pantano, L.; Lauria, A. A3 adenosine receptor: Homology modeling and 3D-QSAR studies *J. Mol. Graph. Model.* **2013**, *42*, 60-72

(27) Perricone, U.; Wieder, M.; Seidel, T.; Langer, T.; Padova, A.; Almerico, A.M.; Tutone, M. A Molecular Dynamics-Shared Pharmacophore Approach to Boost Early-Enrichment Virtual Screening: A Case Study on Peroxisome Proliferator-Activated Receptorα. *ChemMedChem* **2017**, *12*, 1399-1407.

(28) Tutone, M.; Pantano, L.; Lauria, A.; Almerico, A.M. Molecular dynamics, dynamic site mapping, and high throughput virtual screening on leptin and the Ob receptor as anti-obesity target. *J. Mol. Model.* **2014**, *20*, 2247-2257

(29) Phase, version 4.3, Schrödinger, LLC, New York, NY, **2015**

(30) Dixon, S.L.; Smondyrev, A.M.; Knoll, E. H.; Rao, S.N.; Shaw, D.E.; Friesner, R.A. PHASE: A New Engine for Pharmacophore Perception, 3D QSAR Model Development, and 3D Database Screening. 1. Methodology and Preliminary Results. *J. Comput. Aided Mol. Des.* **2006**, *20*, 647-671

(31) Golbraikh, A.;Tropsha, A. Beware of q2!, *J. Mol. Graph. Model.* **2002**, *20*, 269–276

(32) Ojha, P.K.; Mitra, I.; Das, R.N.; Roy, K. Further exploring rm2 metrics for validation of QSPR models. *Chemom. Intell. Lab. Syst.* **2011**, *107*, 194–205

(33) Baldassano, S.;, Liu, S.; Qu, M.H.; Mulè, F.; Wood, J.D. Glucagon-like peptide-2 modulates neurally evoked mucosal chloride secretion in guinea pig small intestine in vitro. *Am J Physiol Gastrointest Liver Physiol.* **2009**, *297*, G800-G805

(34) Baldassano, S.; Wang, G.D.; Mulè, F.; Wood, J.D. Glucagon-like peptide-1 modulates neurally evoked mucosal chloride secretion in guinea pig small intestine in vitro. *Am J Physiol Gastrointest Liver Physiol.* **2012**, *302*, G352-G358

(35) Almerico, A.M.; Tutone, M.; Guarcello, A.; Lauria, A. In vitro and in silico studies of polycondensed diazine systems as anti-parasitic agents. *Bioorg. Med. Chem. Lett.* **2012**, *22*, 1000–1004

(36) Induced Fit Docking protocol 2015-2, Glide version 6.4, Prime version 3.7, Schrödinger, LLC, New York, NY, **2015**

(37) Sherman, W.; Day, T.; Jacobson, M.P.; Friesner, R.A.; Farid, R. Novel Procedure for Modeling Ligand/Receptor Induced Fit Effects. *J. Med. Chem.* **2006**, *49*, 534-553.

(38) Sherman, W.; Beard, H. S.; Farid, R. Use of an Induced Fit Receptor Structure in Virtual Screening. *Chem. Biol. Drug Des.* **2006**, *67*, 83-84.

(39) Guo, Z.; Mohanty, U.; Noehre, J.; Sawyer, T.K.; Sherman, W.; Krilov, G. Probing the alpha-helical structural stability of stapled p53 peptides: molecular dynamics simulations and analysis. *Chem. Biol. Drug Des.*, **2010**, *75*, 348–359

(40) Shivakumar, D.; Williams, J.; Wu, Y.J.; Damm, W.; Shelley, J.; Sherman, W. Prediction of Absolute Solvation Free Energies using Molecular Dynamics Free Energy Perturbation and the OPLS Force Field. *J. Chem. Theory Comput.* **2010**, *6*, 1509–1519

(41) Harder, E.; Damm, W.; Maple, J.; Wu, C.; Reboul, M.; Xiang, J.Y.; Wang, L.; Lupyan, D.; Dahlgren, M.K.; Knight, J.L.; Kaus, J.W.; Cerutti, D.S.; Krilov, G.; Jorgensen, W.L.; Abel, R.; Friesner, R.A. *J. Chem. Theory Comput.* **2016**, *12*, 281-296

(42) QikProp, version 4.4, Schrödinger, LLC, New York, NY, **2015**

Highlights:

- Nonsense mutations originate premature termination codons (PTC) in the mRNA
- PTC are responsible for the production of a not-functional truncated protein
- Translational readthrough inducing drugs (TRIDs) rescue protein production
- CFTR production and functionality can be restored by TRIDs
- Oxadiazoles are small non-toxic molecules with readthrough activity